ALMA MATER STUDIORUM
UNIVERSITÀ DI BOLOGNA

DEPARTMENT OF INDUSTRIAL CHEMISTRY "TOSO MONTANARI"

SECOND CYCLE DEGREE IN

LOW CARBON TECHNOLOGIES AND SUSTAINABLE CHEMISTRY

CLASSE LM-71 - SCIENZE E TECNOLOGIE DELLA CHIMICA INDUSTRIALE

POROUS SEMICONDUCTING POLYMERIC FILMS FOR HIGH PERFORMANCE ORGANIC ELECTROCHEMICAL TRANSISTORS (OECTs)

Supervisor

Prof. Laura Mazzocchetti

Co-Supervisor

Dr. Olivier Bardagot

Co-Supervisor

Dr. Emanuele Maccaferri

Candidate

Alessandra Pistillo

Session II October 2024

Academic Year 2023/2024

Abstract

Organic electrochemical transistors (OECTs) have gained attention due to their low-cost fabrication, biocompatibility, and unique properties such as *high transconductance*, *low operational voltages*, and *mixed conduction.* These attributes make them ideal for bioelectronics applications, particularly in biosensing. Despite these advantages, OECTs face limitations in their kinetic performance, which influences their ability to detect fast biological events and chemical reactions.

This thesis focuses on enhancing the doping kinetic response of OECTs by introducing porosity in the polymer channel. The polymer studied is poly(3-hexylthiophene) (P3HT). The primary hypothesis is that porous P3HT channels, with their increased surface area, would exhibit faster ionic mobility, improving the device kinetic response. Four methods: the breath figure, dry breath figure, and nanoparticle sacrificial template methods, were explored for fabricating porous P3HT films. Among these, the breath figure method proved to be the only effective and reproductible way of achieving porosity, particularly when optimizing the *solvent nature*, the *relative humidity*, the *spin coating technique* and the *concentration of the polymer solution*.

The kinetic performance of the porous films is then analysed using time-resolved Vis-NIR absorbance spectroelectrochemistry. Unexpectedly, the porous films exhibit slower doping kinetics compared to dense, non-porous, films. A likely explanation lies in the increased crystallinity of the dense films, which enhances electron mobility, neutralizing the benefits of higher ionic mobility due to porosity. Additionally, we found that pore arrangement and coverage influence the performance. The linear pore structure shows faster kinetic results than films with a honeycomb-like porous structure.

Even though the porous P3HT films shown slower doping kinetics, the ideal polymer engineering method to fabricate porous films has been identified and mastered. This research is also a starting point for future efforts to improve the morphology of semiconducting polymer films to enhance OECT performance, and derived bioelectronic devices.

Table of Contents

1. INTRODUCTION

In the last decades, the interest for organic electrochemical transistors (OECTs) has increasingly grown due to *their low-cost fabrication* and the numerous advantages such as *low operation voltages*, *mixed conduction properties* (ionic and electric mobility), and *high transconductance*. In particular, compared to inorganic transistor, they show higher signal amplification due to bulk doping. However, they suffer from slower ON/OFF switching. The switching speed of OECTs can be enhanced by tuning the chemical design of the semiconducting polymer composing the OECT channel as well as its morphology. All these features added to *the high flexibility*, *sensitivity*, *selectivity* and *biocompatibility* make OECTs highly desirable for bioelectronics applications[1–3].

The objectives of this work are detailed in section 1.3. Before, motivating this thesis by briefly introducing the operation and potentials of OECTs as well as presenting what is the current state-of-the-art with an emphasis on the concepts and physical parameters required to understand to appreciate this work.

1.1 Organic Electrochemical Transistors (OECTs)

1.1.1 Structure and Working Principle

OECTs are devices able to "transduce" small ionic signals into larger electrical signals under low potential (< 1V)[1,4]. They consist of three electrodes: a *source* (S) and a *drain* (D) electrode, connected by a *channel material* made of an organic conducting or semiconducting polymer (all of them supported by a substrate) and a *gate* (G) electrode immersed in a liquid *electrolyte*.

The working principle of an OECT (Figure 1) relies on the doping state of the conducting or semiconducting channel material: when doped the transistor is ON, when undoped the transistor is OFF[2].

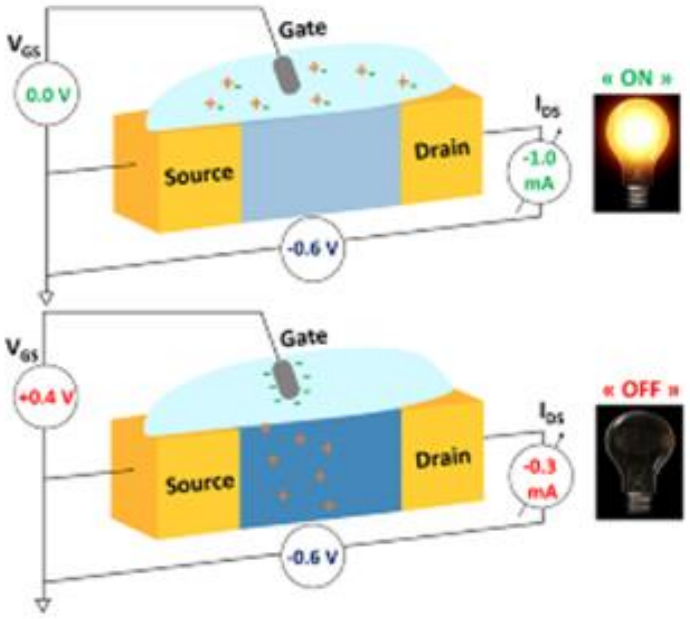

Figure 1. Schematic representation of the working principle of OECTs (reproduced from: [2]).

The ON/OFF state of the transistor is controlled by the *voltage* applied at the gate electrode (V_{GS}). V_{GS} is the *driving force* for ions to move from the electrolyte within the matrix of the channel material, thus causing the oxidation/reduction of the polymer (doping/dedoping). The value of the V_{GS} applied depends on the type of polymer used (conducting or semiconducting) and on the working mode of the transistor: *depletion mode* or *accumulation mode* (Figure 2).

Typically, OECTs with conducting polymers as channel material work in depletion mode. In absence of a gate voltage the polymer is intrinsically *chemically doped* and a current flows between the source and drain electrodes (I_{DS}), so the transistor is ON. Assuming a p-type conducting polymer (such as PEDOT:PSS), by applying a positive gate voltage, positively charged cations contained in the electrolyte will be injected into the polymeric channel, thereby dedoping it and switching the transistor OFF (holes extraction from the channel). In contrast, OECTs with semiconducting polymers (such as P3HT) as channel material work in accumulation mode. Assuming a p-type semiconducting polymer, in absence of a gate voltage, the polymer is intrinsically neutral (dedoped), no I_{DS} current flows between the source and the drain electrodes and the transistor is OFF. However, by applying a negative gate voltage, negatively charges anions contained in the electrolyte will be injected into the polymeric channel, which is then oxidized, thus *electrochemically doped* (holes accumulation), turning the transistor ON.[5,6]

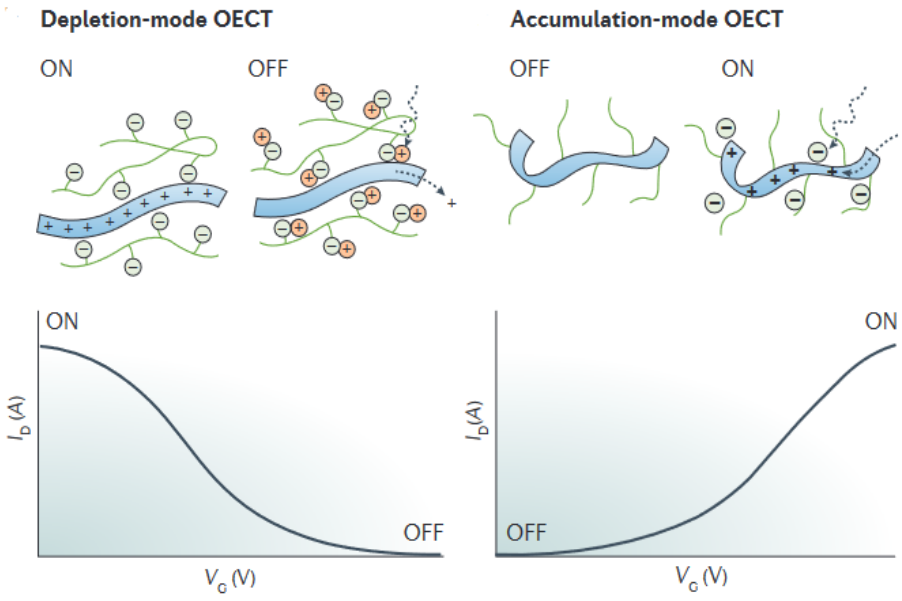

Figure 2. Transfer curves showing (left) depletion-mode OECT and (right) accumulation-mode OECT (reproduced from: [5]).

1.1.2 Advantages of OECTs over Traditional Transistors

Transistors are essential devices for controlling, amplifying, and modulating electrical signals. They consist of three main terminals. *Metal Oxide Semiconductor Field Effect Transistors (MOSFETs)*, a type of traditional transistor, consist of *source*, *drain*, and *gate* terminals. *Bipolar Junction Transistors (BJTs)*, another common type, include *collector*, *emitter*, and *base* terminals. Silicon-based transistors are prevalent[2], although alternatives such as *germanium*, *gallium/arsenide*, and *indium* compound-based transistors are also used. *Organic Electrochemical Transistors (OECTs)* use organic semiconductors as channel material.[7]

A first key difference between a MOSFET and an OECT is in the structure (Figure 3). Indeed, for MOSFETs a solid dielectric separates the gate electrode from an inorganic semiconductor channel material, while for OECTs, the gate electrode is immersed in a liquid electrolyte in contact with an organic semiconductor material forming the channel.[5,8,9]

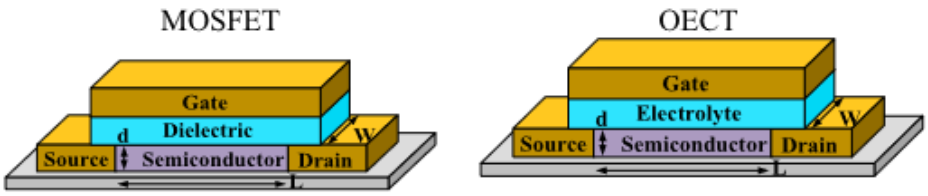

Figure 3. Structures of MOSFETs and OECTs respectively. Reproduced from: [8].

Another fundamental difference between OECTs and *traditional inorganic transistors* like MOSFETs lies in their operational mechanisms. Traditional MOSFETs are based on *field-effect doping*, where a gate voltage modulates the number of mobile electrons (n-type) or holes (p-type) in the semiconductor through a thin insulating layer (*gate dielectric*)[10,11]. While OECTs operating mechanism relies on electrochemical doping, where a gate voltage triggers a flux of ions from the electrolyte into the organic semiconductor channel, controlling its doping state (see 1.1.1). This process leads to *high gate-channel capacitances* up to 9 mF/cm², [8] overcoming the capacitances of MOSFETs high-κ dielectrics. Consequently, OECTs can operate at *very low voltages* (~0.5 V vs. ~2V for MOSFETs)[11] and achieve a geometry-normalized *transconductance* value of 687 ± 91 S/cm[12] which is much higher than that of traditional transistors. The higher transconductance of OECTs is attributed to bulk doping, which occurs throughout the entire thickness of the channel, in contrast to MOSFETs, which rely on field-effect doping confined to the surface. This high transconductance translates into enhanced *sensitivity*, particularly useful for detecting small changes in signals.[3,8,13]

Another important difference is in their *operational speed*. OECTs generally exhibit slower speeds compared to MOSFETs. The response time of OECTs, which is the time for the device to turn ON, is limited by the *ionic circuit*, which is affected by the resistance of the electrolyte and the capacitance of the channel.[5] Additionally, thicker channels, while providing higher capacitance and gain, slow down the device response as the ions have more thickness to go through to entirely (de)dope the channel. Conversely, MOSFETs are generally faster as rely only on almost instant *field-effect*s and *electronic conduction*.[5,14] Indeed, MOSFET, conversely to OECTs, are not kinetically limited by motion of ions and/or charge carriers across hundreds of nanometers of channel thickness.

Despite these differences, OECTs present unique advantages, especially in applications involving biological systems. The low operating voltages of OECTs allow them to detect living cells and other organisms, maintaining their integrity. It also makes low-power consuming

biosensors. Their biocompatibility and flexibility make them suitable for medical devices. The biocompatibility combined with the high transconductance make OECTs advantageous over traditional, rigid inorganic transistors. [2,15]

The Table 1 below summarizes the key differences between OECTs and traditional transistors, emphasizing the unique advantages of OECTs.

OECTs	**Traditional Transistors**
Polymeric materials (soft)	Inorganic materials
Liquid electrolyte	Solid dielectric
Low costs	High costs
Lightweight	Heavy metals
Flexible	Rigid
Biocompatible	Not biocompatible
Slow kinetic	Fast kinetic
High transconductance	Low transconductance

Table 1. Key differences between OECTs and traditional transistors.

1.1.3. Applications

Organic Electrochemical Transistors (OECTs) are employed in a broad spectrum of applications thanks to their ability to transduce small ionic signals into larger electrical outputs as well as their flexibility and biocompatibility, as mentioned in section 1.1.

The most common field of application is certainly *bioelectronics.* OECTs are indeed engaged in measuring cell activity, interfacing with electrically active tissues and organs, and recording electrophysiological signals.[2,5,6,8] They are used for detecting biomarkers like miRNA-21 with high sensitivity reaching low detection limits (2 pM). They are also exploited as biosensors like glucose sensors, achieving micromolar sensitivity through enzymatic reactions.[8,16] In practical use, they can be integrated as *wearable technology* on skin or clothing to detect several *analytes* in sweat, breath, saliva or cell culture media, becoming attractive for *health monitoring*.[2,5,6,8,15,16]

OECTs are also studied for less ordinary application fields such as *neuromorphic computing*. It has been observed that they take part in systems that simulate brain functions, thus bringing advancements in artificial intelligence. This application make them potentially attractive for mimicking complex neural processes.[14,17,18]

Other applications include the integration into *electronic circuits, electrochromics*, *drug delivery systems*, (ion pumps, by amplifying small ion concentration changes) and *energy storage* implementation for supercapacitors and solid-state batteries.[2,5]

OECTs show great promise in various applications; their widespread adoption is currently limited by the slow kinetics of ON/OFF switching, which is linked to the time required for ion transport and channel doping/dedoping processes. To unlock the full potential of these applications, it is essential to conduct fundamental studies in polymer engineering. These studies should aim to **accelerate the doping/dedoping kinetics** within the channel, enhancing the overall switching speed. By addressing these challenges, OECTs can transition from promising concepts to practical, real-world technologies.[5,19]

The next section will present the state-of-the-art and the proposed methodology to address these limitations via a fundamental study to foster the applicative use of OECTs for energy and health applications.

1.2 State-of-the-art of Organic Electrochemical Transistors (OECTs)

The first organic electrochemical transistor (OECT) dates back to the 1984, when White and coworkers developed a device, consisting of two gold electrodes and a polypyrrole (PPy) channel, able to conduct both electrons and ions[2,20]. Since then, many studies have been carried out, leading to the development and improvement of these devices, which, as mentioned in section 1.1, are nowadays very versatile for a wide range of applications in several fields such as *wearable electronics*, *electronic circuits, electrochromics, drug delivery systems* and *energy storage*. Although, in order to produce Organic Electrochemical Transistors (OECTs) that can be practically used in these applications, it is essential to understand how to control and enhance their performance. Two main factors describe an OECT efficiency: the *transconductance* and the *kinetic*. They both depend on several factors, among which an important role is played by the features of the polymeric channel material.

Ideally, an efficient OECT would exhibit high transconductance and fast kinetic simultaneously in order to amplify small ionic signals with high sensitivity while enabling rapid, real-time responses in applications like biosensing, neuromorphic computing, and health monitoring. However, these two parameters often conflict with each other, making it challenging to accomplish this ideal case.[18] The following sections define these terms and present the current state-of-the-art.

1.2.1 Transconductance

The *transconductance* (g_m) is the modulation of the I_{DS} current flowing through the semiconductor channel material (detected output signal) triggered by a variation of the V_{GS} gate voltage (Equation 1) (Figure 4). In case of a biosensor, a variation of V_{GS} is for instance caused by a sensing event (presence of the targeted analyte). In other words, g_m quantifies the overall signal amplification of the transistor. Our goal is to maximize g_m as the higher it will be, the higher the sensitivity of the sensor, and so the lower the detection limit will be.

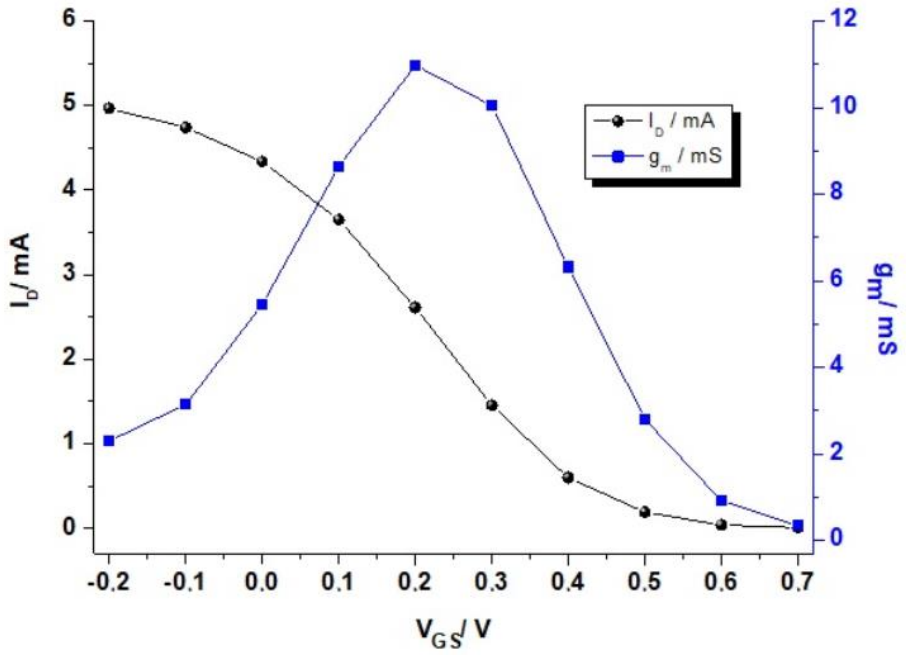

Figure 4. Example of transfer curve (black) and transconductance (gm) (blue) of an OECT in depletion-mode operation (reproduced from: [2]).

It is mathematically defined as:

$$g_m = \frac{\partial I_{DS}}{\partial V_{GS}} = \frac{W}{L} \cdot d \cdot \mu \cdot C^* \cdot (V_{Th} - V_{GS})$$

Equation 1

The transconductance is crucial for the signal amplification and sensitivity of OECTs. It depends on several factors: i) the *geometry* of the transistor channel, [22] which in turn influences its *width* (W), *length* (L), and *thickness* (d), ii) the *mobility of charge carriers* (μ)[18] iii) the *volumetric capacitance* (C*)[23] of the channel material, which is the material ability to store electric charge per unit volume and iv) the *threshold voltage* and the *gate voltage*[14] (Equation 1). Therefore, it is possible to enhance the transconductance controlling these parameters.[18,19,21,24] For instance, a recent study have demonstrated that acting on the transistor geometrical configuration by modifying the traditional planar OECT design into a vertical one (vOECT) can lead to higher transconductance value up to 275 mS,[22] while standard planar OECTs generally output g_m in the range of 1-80 mS.[1,21,25] The vertical configuration creates extremely short channel lengths (L about 60 nm[22] *vs.* 5-100 μm typically)[1,18,23], which is how significantly higher transconductance are achieved.

Nonetheless, further optimization of the transconductance is not trivial as the cited parameters interconnected. For instance, one could improve g_m by increasing the volumetric capacitance (C*). However, a high C* means a better ion diffusion in the entire 3D channel material (and not just the surface) and an increased ionic charge storage, Unfortunately, this typically cause structural and energetic disorder within the polymer channel, thereby reducing the *charge carrier mobility* (μ) and, as a consequence, the overall *transconductance* and *kinetics* of the device.[19] A fine balance between C* and μ should hence be achieved by polymer engineering. In addition, ionic and electronic transports, on which the transconductance depends on, can cause irreversible micro- and nano-scale polymer structural changes over time, potentially lowering down the device long-term *stability*. [1,19,26,27]

To deal with these limitations and optimize conflicting OECT parameters, one can vary the *polymerization methods*,[18] the *polymer molar mass*,[19] and its *processing conditions*[18] as well as the channel *morphology*[19] and the choice of the *electrolyte* (*ions/counterions* and *solvent)*[28] (see

1.2.3 Polymers as Channel Materials for details).

The literature of OECTs is rich in studies focused on improving the transconductance, although it is poorer concerning the enhancement of the kinetic performance – a yet critical criterion as explained below.

1.2.2 Kinetic performance

The kinetic performance of an OECT refers to how quickly the device can switch between ON and OFF states. This is fundamental for some applications dealing with biosensing, detecting neural signals and neuromorphic computing as the increased speed of the device improves its sensitivity. For instance, if the device cannot switch fast enough, it will not be able to detect fast biological events or chemical reactions that occurs in a short time range.[21,24]

Specifically, the **kinetic performance** is the result of the *response time* (τ), which is the time associated to the *doping/dedoping rate* of the polymeric channel material and resulting I_{DS} current generation. The **response time (τ) is quantified by** the ***ion transit time*** (τ_i) and the ***electronic transit time*** (τ_e)**.** The ion transit time depends on the *resistance of the electrolyte* and the *capacitance* of the channel.[19] While the electronic transit time depends on the carrier mobility (μ), the drain-source (V_{DS}) voltage applied, and the length the charge carriers travel (l). [19]

Ion migration is traditionally *slower* in OECTs, representing a limiting factor. Indeed, ion movement imposes an upper limit on switching speed, similar to the delay in a resistance-capacitance (RC) circuit, typically in the range of 1–100 µs. However, recent advancements have reduced the response time to values as low as 20 µs.[2,29] On the other hand, the doping/dedoping rate is related to the *chemical nature* of the polymer itself, to the *morphology* and *thickness* of the polymer channel and again to the *ionic mobility* within the polymer.[2,21,30]

Nevertheless, Inal and coll. report two possible kinetic behaviors in OECTs: i) the *monotonic relaxation* and ii) the *spike and recovery*. The monotonic relaxation occurs when the *electronic transport* is faster than the *ionic* charging, I_{DS} relaxes monotonically until it reaches its steady-state value (Figure 5i). If the "*spike and recovery*" behavior verifies, then the electronic transport becomes the limiting factor and I_{DS} displays a spike beyond the final steady-state current before the exponential relaxation to the final current (Figure 5ii).[3,24]

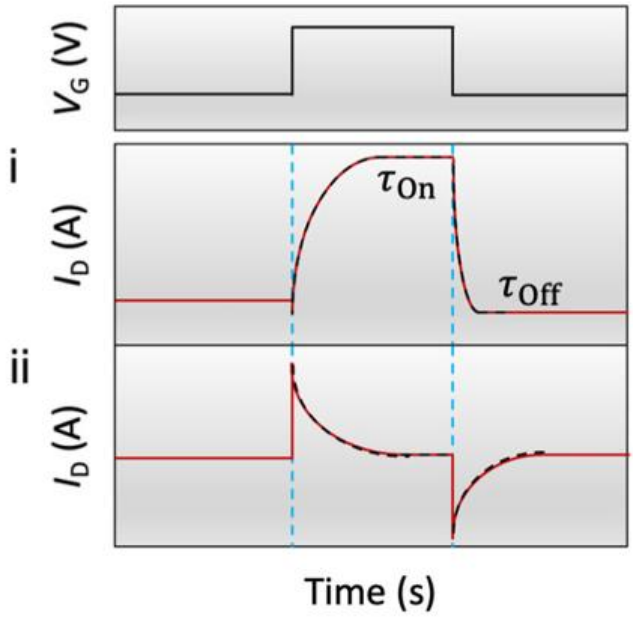

Figure 5. The transient characteristics of an OECT. ID in response to a square VG pulse is measured (VD constant). (i) Monotonic relaxation of ID towards the steady-state value, (ii) or a ''spike and recovery'' behaviour (reproduced from: [21]).

Other parameters can affect the **kinetic performance** such as the *geometry* of the device, the type of *electrolyte*, the *thickness* of the channel material (<1µm) and as before mentioned the physical and chemical *properties of the polymeric channel material* (*e.g. chemical structure* of the polymer, channel *morphology*).[2,13,19,21] The latter will be discussed in section 1.2.3.

This is confirmed by several studies and innovations. An example is the work of Spyropoulos et al., which developed an internal ion-gated electrochemical transistor (IGT) displaying improved device kinetic.[31] By incorporating mobile ions in the channel material (*e.g.*, D-

sorbitol) that acts as an ion reservoir and conductivity enhancer, the device response is significantly reduced (31.7 μs *vs.* 191.2 μs without).[24,31]

Chen et al. studied how changing the side-chain structure in ethylene glycol (EG)-substituted polythiophenes affects OECTs performance.[32] They discovered that the EG side-chain speeds up the doping process due to enhanced ion transport in the film. Additionally, having a polar functional group (like oxygen) distant from the polymer backbone helps improving the ion movement and device switching speed.[24,32]

Finally, a key role in the OECT kinetic is played by the choice of *electrolyte*, specifically the anion involved. The *size* and *hydration state* of the *anion* determine the speed of the device. It has been reported by Ginger and coll. that *larger anions*, such as *hexafluorophospahte* (PF_6^-) and *triflimide* ($TFSI^-$), enter the polymeric film (P3HT in this study) with low hydration (less solvating water molecules dragged in), allowing faster doping/dedoping and *quicker* current modulation (Figure 6). They managed to reach steady-state conditions (ON) in less than 30s.[28] Conversely, *smaller anions* like *chloride* (Cl^-) and *perchlorate* (ClO_4^-), which are more hydrated, require more energy to move from the electrolyte into the bulk of the polymer matrix, resulting in *slower* current modulation times (>200 s). This kinetic difference is due to the energy associated with *solvation changes* and the *interaction* between the anion and the polymer.[28,33,34]

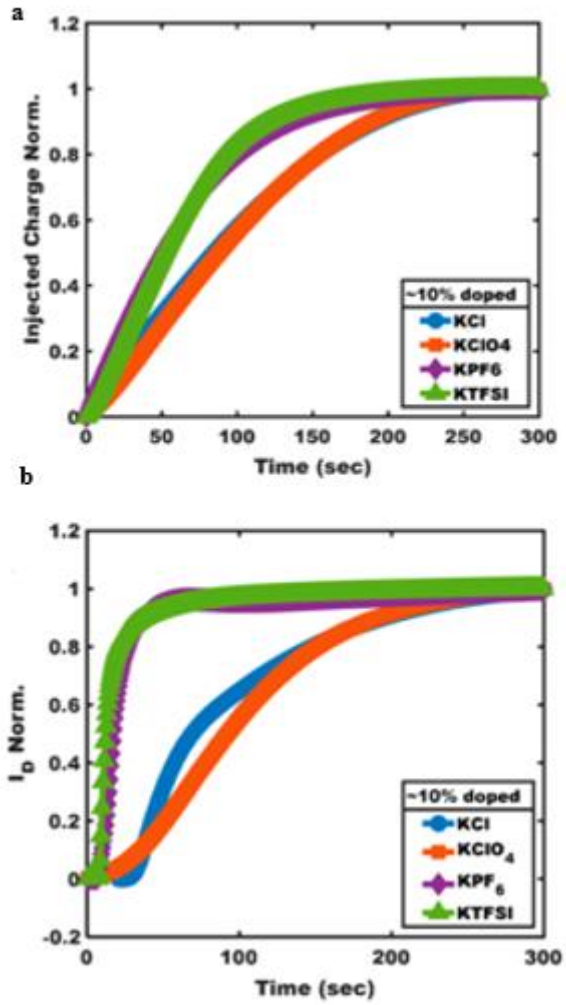

Figure 6. a) Normalized charge injected into the film during a doping step. b) Normalized transistor current over time for four different ions(reported from: [30]).

1.2.3 Polymers as Channel Materials

Polymers used as channel materials in OECTs need to possess both electronic and ionic conductivity properties, which are not common to all polymers. A particular class, known as **Organic Mixed Ionic-Electronic Conductors (OMIECs)** fulfills this requirement. Among these, π-conjugated polymers are often utilized due to their delocalized π-electrons, which enable the conduction of electronic carriers. These polymers are semiconducting and electronic charge transport is allowed along and between polymer chains (carrier hopping). The structure of these polymers can be chemically tailored to better suit the applications (*e.g.*, favor more ordered molecular packing when casted in film). They can also be doped to enhanced the

electronic transport properties. *Electrochemical doping* is the generation of the conductive state is the result of the V_{GS} voltage that is applied.[13] Hence the semiconducting polymers, used as channel materials, are classified as **p-type** (hole transporting), the material is positively doped and **n-type** (electron transporting), the material is negatively doped. P-type polymers are more commonly used in OECTs due to their *higher conductivity, stability,* and *easy processing*. N-type polymers have lower stability and electron mobility, limiting their performance. [2,35]

The most common p-type polymers include the family of *thiophenes* (*e.g.*, PEDOT and its derivatives), and *D-A conjugated polymers*. N-type polymers include *NDI-based polymers*, *IID-BDF-based polymers*, *BTI-based polymers* and *DPP-based polymers*.[2,35] Some examples are shown in Figure 7.

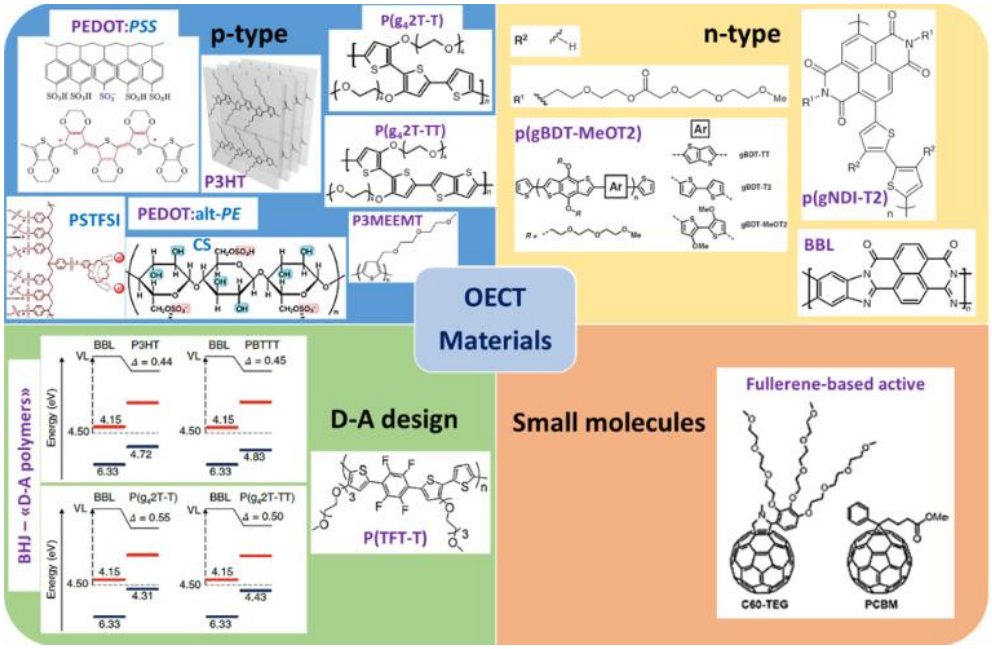

Figure 7. Summary of representative OECTs channel materials.[2]

The performance of an OECT is highly influenced by the type of polymer used as channel material. A key advantage of these materials lies in the ability to tune their *chemical structure* and *morphology*, enabling the optimization of the desired device performance.[18,35]

The introduction of ethylene-glycol (EG) side chains to the semiconducting material improves the ionic transport properties.[36] These polymers consist in a *π-conjugated backbones*, which allows electronic charge transport and *hydrophilic side chains* that allows efficient ion transport. The length of the side chain has been proved to play an important role too.[13,35,37]

In parallel, it has been reported that acting on the *polymer backbone* copolymerizing structural units with different functions can affect the device efficiency.[19] Copolymers composed of monomers from the poly(3-hexyl-thiophene) (P3HT) and poly(thiophene-3-hexylsulfonate) (PTHS) combine the strengths of the two units, resulting in high volumetric capacitance (C* > 100 F cm^{-3}), high hole mobility (μ=1.7 × 10^{-2} cm^2 V^{-1} s^{-1}), a low threshold voltage (-0.15 V), and a better ON/OFF ratio compared to PTHS alone. This design approach not only improves the performances over PTHS, but can also enhances the performance of other *hydrophobic* materials that struggle with *ion transport* and *swelling* in aqueous environments.[35]
Alternatively, modifying the *morphology* of the OECT channel can significantly enhance the kinetic performance. *Dense morphologies* usually benefit the electrical conductivity due to improved *molecular packing* and *crystallinity*, but often impede efficient ion migration. In contrast, *porous morphologies* facilitate better ion transport by providing more accessible pathways for doping and de-doping processes. This leads to improved doping levels, *faster response times*, *higher capacitance* and *higher transconductance*.[33,38]

This work focuses on a p-type polymer of the family of thiophenes, the **poly (3-hexyl thiophene) (P3HT)** (Figure 8). It is a vastly studied polymer in the field of organic electronics and commonly considered as the reference p-type material for conducting fundamental studies for the development of new organic technologies (photovoltaics, thermoelectricity, transistors, etc). Despite its *low solubility* in common solvents, the *hydrophobicity* of its alkyl side chain (lowering ion uptake when using an aqueous electrolyte), and its *high oxidation* potential negatively affecting the conductive properties,[2] P3HT displays competitive advantages for fast transfer to industry such as *easy fabrication*, *low-cost*, *easy processability*, and *environmental* and *thermally* stability.[2,19] Therefore, P3HT is the workhorse for validating a novel proof-of-concept and implementing a new methodology in a laboratory before moving to more complex and expense polymers.

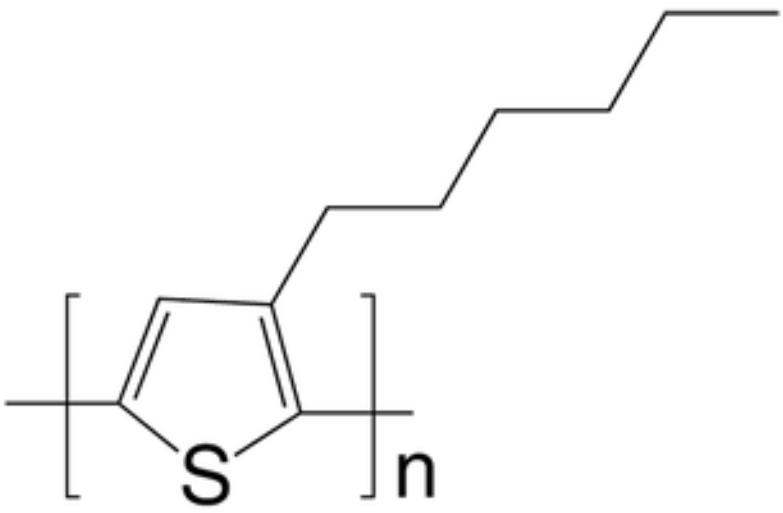

Figure 8. Molecular structure of poly (3-hexylthiophene) (P3HT).

This work specifically **aims at the enhancement of the kinetic performance of an OECT using P3HT as the channel material**. Unlike a part of the current research, which focuses on altering the chemical design of P3HT,[32,36,37] our approach is to modify its film morphology by **introducing porosity**. Creating a porous structure could potentially **increase *ionic mobility*** through the channel (τ_i), and **increase *ionic uptake*** (C*) with **minimal disruption of the electronic conductive pathways** (τ_e and μ), consequently improving the **kinetic performance** of the OECT.

In the course of the study, it is essential to consider that, like the rest of polymers, P3HT presents both *crystalline (ordered)* and *amorphous (disordered) regions*.[34] Ions are thought to preferentially occupy amorphous regions, while polarons are proven to form preferentially in crystalline regions at low V_{GS} due to the lower oxidation potential compared to amorphous regions. This distribution significantly affects the *speed of ion injection,* and thus the overall doping/doping kinetics of the polymer channel. Controlling the channel morphology is therefore critical for a rational improvement of the ON/OFF kinetics of OECTs. For instance, the study by Bischak and coll. shows that balancing crystalline and amorphous regions to a 75:25 crystalline-to-amorphous ratio for a P3HT films allows to achieve *faster ion injection kinetics* than both purely crystalline and purely amorphous films.[28,33]

This relationship between morphology and ion kinetics introduces a bottleneck to overcome: increased crystallinity enhances *electronic charge mobility* but often *impedes ion transport*.[28] Therefore, a *fine balance* between the charge carrier mobility and ion transport must be found to achieve a faster kinetic response while maintaining a high signal amplification (g_m). [1]

1.3 Objectives

As mentioned in section 1.2.2, while the research mainly focused on enhancing the transconductance to improve OECT performance, understanding how to optimize kinetic performance remains still challenging. The ultimate goal in bioelectronics would be to develop faster devices (currently in the ms range and ideally down to the µs range) while maintaining high transconductance and long-term stability.

The general objective of the thesis is enhancing the doping kinetic performance of an organic electrochemical transistor (OECT) by using a highly porous P3HT film as channel material. The research hypothesis is that the introduction of porosity in the P3HT film increases the film surface area in contact with the electrolyte. Therefore, when the transistor is ON, anions can penetrate the film thickness more easily compared to the equivalent dense film, oxidizing more quickly the polymer. This hypothesis is supported by a three recent articles published from 2020 to 2024.[39–41] Compare to existing literature, the **innovative goal is to control the pore size (from 200 nm to 800 nm)**. In addition, the aim is to elaborate a film with a **complete pore coverage** with pores **homogeneously distributed** across the film.

Hence, the **first sub-goal** of the internship consists in the preparation of **reproducible** and **homogeneous porous-P3HT** films (abbreviated, p-P3HT) with **full pore coverage**. Several methods are exploited, among which the Breath Figure (BF) shows the best results. In the attempt to achieve that, the methodology is to optimize the deposition conditions required to induce BF (discussed in section 2.1). The **second sub-goal** consists in the identification of a **correlation between the porosity and the (ideally faster) doping kinetic of p-P3HT film** compared to dense-P3HT (reference, abbreviated d-P3HT), employing time-resolved spectroelectrochemical Vis-NIR absorbance measurement (discussed in section 3).

2. METHODOLOGIES

This section discusses the **methodologies** used to accomplish the objective of this thesis. Hence, the methods to prepare reproducible full-pore coverage P3HT films: (i) Breath Figure, (ii) Dry Breath Figure and (iii) Nanoparticle Template methods as well as the analysis used to study the doping/dedoping kinetic of these films.

2.1 Breath Figure Method

Breath Figure (BF) is a *simple* and *adjustable* technique, carried out under *mild conditions*, for preparing porous films. It consists of spin coating, in a humid environment (RH >60 %), a polymeric solution prepared in a volatile solvent. First, the polymeric solution is dropped on a substrate, then, due to its volatility, the solvent starts to evaporate, cooling down the film. This causes the formation of water vapor droplets that grow and organize in an array arrangement. The subsequent aqueous droplet evaporation results in the formation of a porous polymer microstructure, each droplet creating one pore (Figure 9).[42–44]

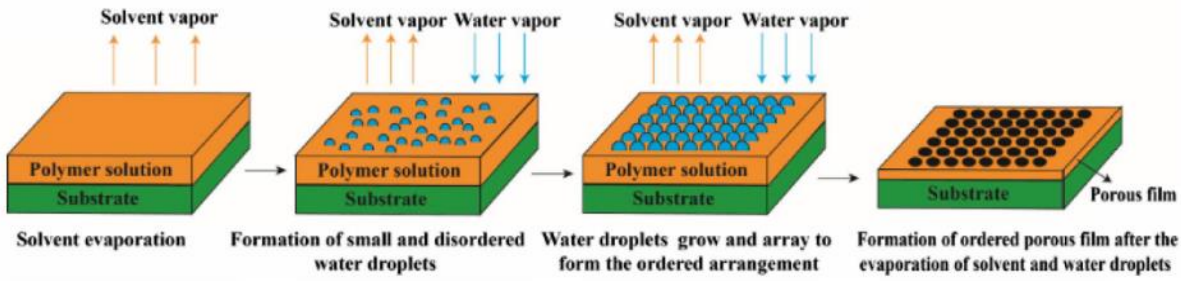

Figure 9. Schematic representation of the BF. Ordered porous films of biomass-based polymers by breath figure: a review (reproduced from: [40]).

Breath figure (BF) can be classified into two methods: *dynamic* and *static* (Figure 10). In the *dynamic method*, water vapor is conveyed over the substrate using airflow, which makes it possible to control the *flow rate* and *humidity* more accurately, thus affecting pore formation. Additionally, gas flowing with high velocity can change the shape of pores from circular to

elliptical. Conversely, the *static method* relies on the ambient environment to provide humidity, with the solvent naturally evaporating. This reduces the disturbances and allows the production of more uniform films.[45,46]

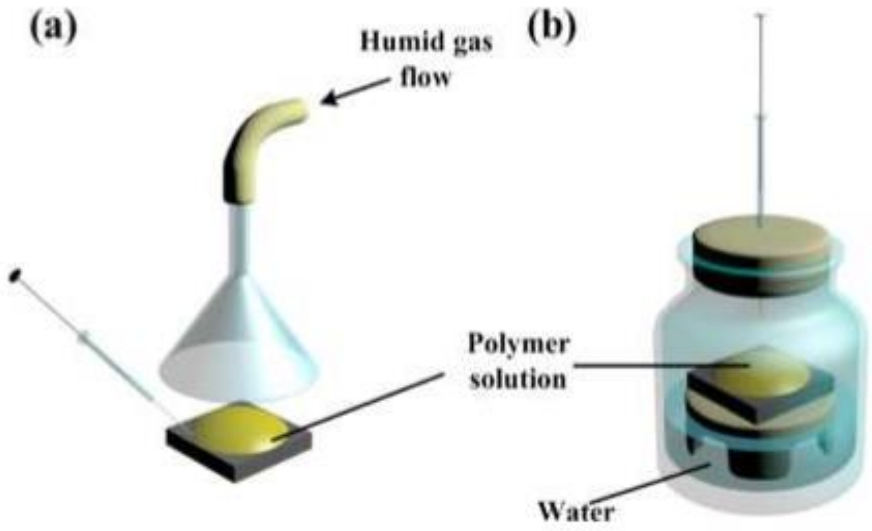

Figure 10. Conventional BF methods. (a) Dynamic and (b) static BF processes (reproduced from: [39]).

The *regularity*, the *size* and the *shape* of pores as well as the spacing between pores are influenced by the *chemical structure*, the *molar mass*, and the *concentration* of the polymer used, and other experimental variables such as *solvents*, *substrates*, *humidity*, *temperature* and *gas flow velocity* in the case of dynamic BF. In this study, we have tested all these parameters to achieve the desired P3HT-film morphology. The methodological details to master about each parameter are introduced in the sub-sections 2.1.1-5 below. Based on this, the corresponding results achieved are presented and discussed in section 3.

2.1.1 Relative Humidity

The relative humidity (RH%) is defined as:

$$\mathrm{RH} = \frac{p}{p_s} \cdot 100\%$$

Where p is the partial pressure of water vapour and p_s is the saturated vapour pressure of water. Higher relative humidity will lead to higher pressure and a faster growth rate .

Controlling the *relative humidity percentage* (RH%) during the BF process is crucial for ensuring the creation of an orderly porous array as well as for determining the pore size. If the relative humidity is too low, it is difficult for the water droplets to nucleate and arrange in an orderly way. On the contrary, if the relative humidity is too high, the water droplets grow up very fast, causing the neighbour water droplets connected to each other hard to form a *regular array* with a smaller inter-pore distance. The threshold value of relative humidity depends on the *polymer* and *additives* used. It is lower if the water droplets are very stable. Besides that, as shown in Figure 11, the higher is the RH, the faster will be the water droplet growth rate, thus the pore size.[43,45]

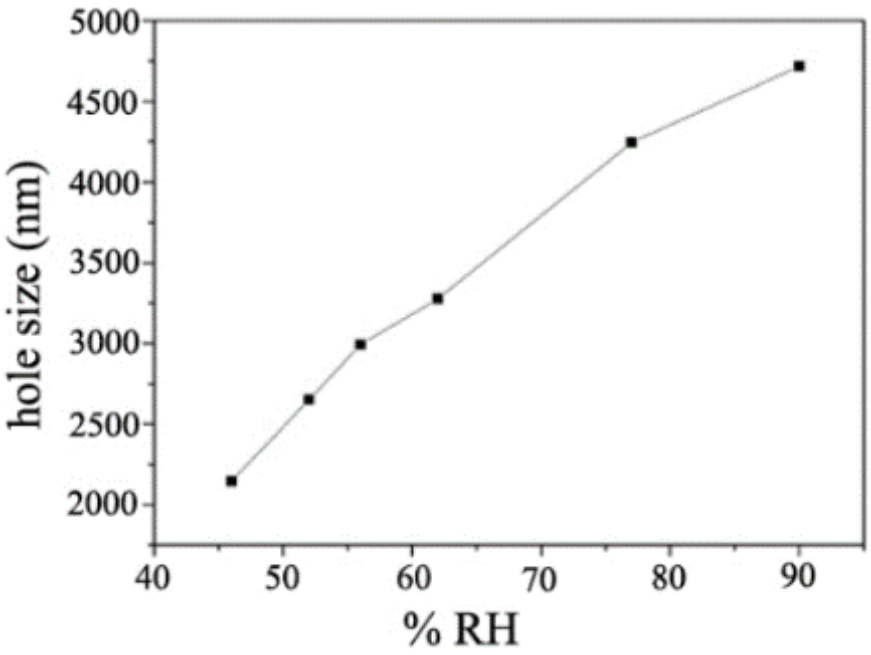

Figure 11. Curve of the pore size of PS honeycomb films versus the relative humidity (reproduced from: [41,54]).

At low humidity (< 46%) or high humidity (> 90%), it is very unluckily to obtain an ordered porous structure due to the lack of water or, at the contrary, the presence of too many droplets condensing on the surface of the polymer coalesce with the adjacent water droplets.[47]

In this study, the **static BF method is used**. In order to create the humid environment, a beaker containing water is placed on a hot plate (~100°C) inside a closed chamber. After a sufficiently period of time, the air in the chamber is saturated by water vapour, (see 3.1 P3HT porous films for more details).

2.1.2 Temperature

The *temperature*, which correlates to the relative humidity and the room pressure ($\Delta p \propto \Delta T^{0.8}$), is another parameter affecting the pore size. In general, high temperatures cause the formation of *larger pores*. When the temperature difference (ΔT) between the solution and the atmosphere increases, water condensation is faster, allowing bigger pore formation. On the contrary, when the temperature difference between the surface and atmosphere is small, the water droplet size increases during nucleation is slower, resulting in smaller pore size. The small ΔT is usually due to the low vapour pressure, which slow down the solvent evaporation and generates higher surface temperature.[45,47]

Besides the pore size, the temperature may also affect the pore distribution. Depending on the type of polymer and concentration, *honeycomb structures* can be obtained in a certain temperature range. Higher temperature in this range allows the *pore size distribution* to became *narrower*.[47]

2.1.3 Solvent

The *solvent* influences the water droplet formation phase in the breath figure process, which is why solvent selection is so important. Key solvent properties, including *thermodynamic affinity* with the polymer, *boiling point, water miscibility* and *evaporation time*, all influence the development of the honeycomb structure.

First, it is important to take into consideration that, since BF method relies on water condensation onto the polymeric film, if the boiling point of the solvent is higher than the one of water (100 °C at atmospheric pressure), water will not be able to condensate on the film and the process will not start at all. The *solvent evaporation speed* slows down as the boiling point of the solvent increases. Therefore, an *organic solvent* is generally employed due to the *higher volatility*.[48]

When the polymeric solution is coated on the substrate, the solvent absorbs a lot of heat, which causes its evaporation and lowers the solution temperature above the ambient temperature. This drop of temperature creates the perfect environment for water droplet condensation. As the solvent evaporates, the *viscosity* of the solution increases and the movement of the water droplets is limited. When the temperature of the solution is above the dew point, the water droplets stop growing and the water droplets evaporate, causing the pore formation. During the evaporation process, which takes several minutes, the *positions* of the droplets cannot significantly change, but the shape of the pores evolves due to the residual solvent, which gives enough fluidity to cause the pores modification. [43,49]

In general, the solvent *evaporation speed* should be slow enough to ensure the right deposition space and time for water *condensing, sinking,* and *aligning*. Although, depending on the pore size desired, the evaporation time must be adjusted by changing the spin coating speed. To obtain a small pore size diameter (nm range), a fast evaporation rate is required. [45,48]

Besides the solvent volatility, it is necessary to consider other factors, such as the water-miscibility. In order to facilitate pore formation, a *water-immiscible solvent* is selected, so that the dissolution of water droplets into the polymeric solution is prevented. This is also associated to the *interfacial tension* between the solvent and/or the solution and water, which affects the porous films structure itself. Indeed, the water droplets could sink into the polymer solution, forming multilayer honeycomb films. This particularly occurs if the density of the solution is smaller than water, otherwise a monolayer honeycomb films is obtained.

The mechanism of the layers formation can be explained by the *interfacial energy* between the water droplets and the organic solvent. The *interfacial energy balance* (z_0) is defined as:

$$z_0 = z/R = (\gamma_w - \gamma_{w/s})/\gamma_s$$

where z is the distance between the droplet centre and the air/solution interface; R is the droplet radius; $\gamma_{w/s}$ is the interfacial tension between water and solution; γ_w and γ_s are the surface tension of the water and the solution, respectively (Figure 12).

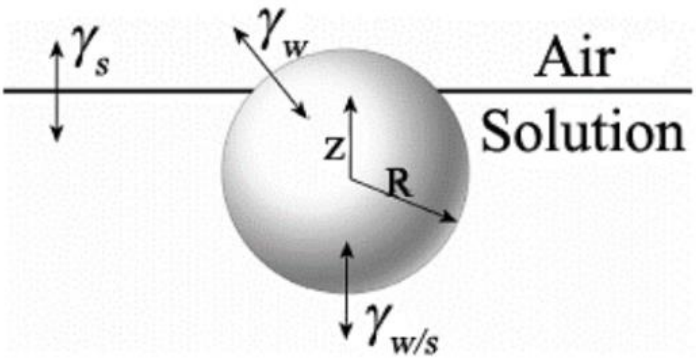

Figure 12. Schematic view of a spherical water droplet at the air/solution interface (reproduced from: [54]).

If the *interfacial energy* (z_0) is in the range of ± 1, only one layer of droplets stays between the air and solution interface, forming monolayer ordered structures. If $z_0>1$, the droplets sink into the solution, forming multilayer films. Finally, if $z_0 < -1$, water droplets are not able to remain at the interface or in the solution, so no ordered structure is obtained. However, the formation of monolayer or multilayer films is also related to the polymer solution thickness, which is why at the edge of the polymer solution, monolayer films is more likely to form considering that the deposition space is not big enough for more layers of water droplets. Since the *surface tension of water* (72,75 mN m^{-1}) is greater than that of organic solvents (20−30 mN m^{-1}), water droplets do not spread on the surface of organic solvents.[45,47,48]

2.1.4 Concentration

The polymeric solution plays a critical role in the Breath Figure (BF) process, influencing the formation of the honeycomb structure. Polymer *concentration* is particularly important in determining the *stability,* the *size* and *arrangement* of water droplets. When the concentration is too *low*, there is insufficient solute to stabilize the droplets, resulting in coalescence and disruption of the pattern. Additionally, at low concentrations, the polymer precipitation is slow, creating weak, thin protective layers around the droplets, thus leading to non-uniform pore formation. In extreme cases, due to the lack of solute, the film can become discontinuous. Conversely, at *high polymer concentrations*, the solution higher viscosity can impede the self-assembly of water droplets, leading to a disordered pore arrangement. [42,47]

The relationship between *concentration* and *pore size* is influenced by the polymer's properties and casting conditions. Higher concentrations increase the *viscosity*, which slows down the

water droplet growth and accelerates polymer precipitation at the water-polymer interface, resulting in smaller pores.[45,49]

Henry's law can also explain this, the vapour pressure of the solvent decreases as the solute concentration increases:

$$\mathbf{P = P_0 (1 - X_B)}$$

Where P and P_0 are the vapour pressures of the solvent in solution and the pure solvent, respectively, and X_B is the mole fraction of the solute. A *higher concentration* lowers the solvent vapour pressure, which slows *evaporation speed* and raises *the surface temperatur*e. The *smaller temperature difference* between the surface and the atmosphere reduces the rate of droplet growth during nucleation, leading to *smaller pores* (see 2.1.2 Temperature). Thus, the polymer concentration, combined with the solution structural and physical properties, has a significant impact on the final pore size and arrangement in the BF process. [45,47,49]

2.1.5 Substrate

The *substrate* influence the *formation, size* and *arrangement* of pores in the honeycomb structure in BF process. Several factors related to the substrate directly affect the *water droplet nucleation* and the subsequent pore array, such as the *material type, thickness, mass, surface energy*, and *wettability*.

Substrate thickness and *mass* act on the *heat transfer* between the polymer solution and the substrate. A thicker or more massive substrate slows down the heat transfer, making it difficult for water droplets to condense and form on the polymer surface. The BF process relies on a cold surface (substrate) for the facilitation of water condensation. Nevertheless, a slower heat transfer reduces the efficiency of droplet formation, resulting in fewer or less uniform size of pores. Additionally, if the substrate is too thick, the *slower cooling effect* may lead to poor droplet stability, causing *disordered pore* arrangements.[45]

Surface energy and *wettability* of the substrate are also determining in the final pore morphology. Substrates with higher surface energy boost the *ordering* of the polymeric solution and consequently the formation of long range ordered pores. On the other hand, a substrate with good wettability facilitates the *interaction* between the polymer solution and the surface of the substrate, which results in more *regular* and periodic pore arrangement. *Hydrophilic* substrates,

in particular, improve water droplet nucleation, forming more uniform pore sizes and enhancing the pore's density. While hydrophobic substrates tend to form irregular patterns. For instance, hydrophilic surfaces like mica have been shown to generate more organized pores than glass or other less hydrophilic materials.[43,45,47–49]

Finally, it has been reported that the substrate material also has a role in the solvent *evaporation rates*, which can affect the self-assembly of droplets (see section 2.1.3 Solvent). The *interaction* between the *solvent* and the *substrate* governs the wetting ability of the polymer solution, which in turn affects the structure of the honeycomb pores. For example, chloroform, a commonly used solvent in BF, is able to generate honeycomb structures on various substrates, including silicon wafers, because it is less sensitive to substrate changes compared to other solvents. However, other substrate-solvent interactions may vary significantly and affect the final pore size, shape, and regularity.[47–49]

2.2 Dry Breath Figure Method

The *Dry Breath Figure* method is a less common alternative to the traditional Breath Figure technique for fabricating porous polymeric films. While the classic Breath Figure requires a high-humidity environment to facilitate the condensation of water droplets forming a honeycomb pattern, the Dry Breath Figure operates under dry conditions (relative humidity < 40%). Hence, this method creates porous structures by controlling water evaporation in low humidity environment. Compared to the traditional Breath Figure method, the porous films exhibit more defects in hexagonal packing due to the faster evaporation of the solvent during spin coating. [50,51]

To mimic the humid environment, water is added to the prepared solution, which should possess precise features. The *solvent*, in particular, must have two main characteristics, it must be *water-miscible* to allow the interaction between the solvent and added water, and it must be able to dissolve properly the polymer. On the other hand, the polymer must be *immiscible* with water to prevent mixing with the water droplets that form on the film surface. This balance is essential for creating the desired porous structure during the evaporation process. [50,51]

Nevertheless, other parameters such as *amount of water* added to the solution, polymer *molar mass*, *concentration* of the polymeric solution and *speed* of the *solvent evaporation* may affect the *pore size* (from hundreds of nanometres to several micrometres) and the *pore arrangement*. Bigger pores can be achieved adding higher *water amount* or decreasing the *spin coating speed*. The latter, specifically, act on the pore size because of its influence on the *evaporation rate*. Faster spin coating speeds cause faster solvent evaporation and *effective surface cooling*, which means that the water droplets do not have the time to grow any further, forming smaller size pore arrays. [50,51]

Besides the pore size, it is important to make few considerations about the pore arrangement. Even if smaller contents of water allow obtaining *smaller pore size*, it could also results in a bad pore packing. In contrast, increasing the water content produces a more well-ordered honeycomb structure, but at the expense of larger pore sizes. Similarly, when *low molar mass*

polymers are employed, the viscosity of the solution will be low, making it very hard to obtain well-ordered pores, because the solution cannot prevent the coalescence between condensed water droplets. Therefore, higher molar masses are favoured. For the same reason *higher concentrations* are preferred, which make the solution viscous enough to prevent the coalescence phenomenon as well as the mixing of water with the polymeric solution. [50,51]

In conclusion, as previously mentioned, the Dry Breath Figure is not commonly employed for the preparation of porous polymeric films and it has not been applied to the fabrication of p-P3HT films, the polymer considered in this study. Therefore, its implementation represents a significant technological challenge with a potentially high impact.

2.3 Nanoparticles Sacrificial Template

The *nanoparticle template method* is a technique typically used in nanofabrication to create porous materials with highly controlled structures. This method involves using nanoparticles as templates to shape other materials, deposited around or between the nanoparticles. Once the desired structure is achieved, the nanoparticles are removed, leaving behind a porous framework. Various casting method can be used, however, this study employs the spin coating (see 2.4 Spin-Coating), because no chemical treatments on the surface is needed, unlike other methods, and because it allows a *uniform nanoparticles distribution* over a wide area, which results in a uniform pore distribution. The **advantage** of the nanoparticle sacrificial template technique resides mostly in the ability to control **pore size** down to the **nm range** and **distribution**. Indeed, the pore size can be controlled by tuning the *nanoparticle size* during their synthesis, while the pore distribution is influenced by the initial solution *concentration* and by the *spin coating speed*.[52–54]

The nanoparticle template method applied in this work for the achievement of p-P3HT films, involves i) the use of Poly(methyl methacrylate) (PMMA) nanoparticles (d~100nm), which are spin coated on a ITO glass substrate, ii) the use of a polymeric solution of P3HT in xylene, spin coated on the nanoparticle layer and iii) a bath of Ethanol (CH_3CH_2OH) to dissolve the nanoparticle layer and leave a porous thin film behind (Figure 13).

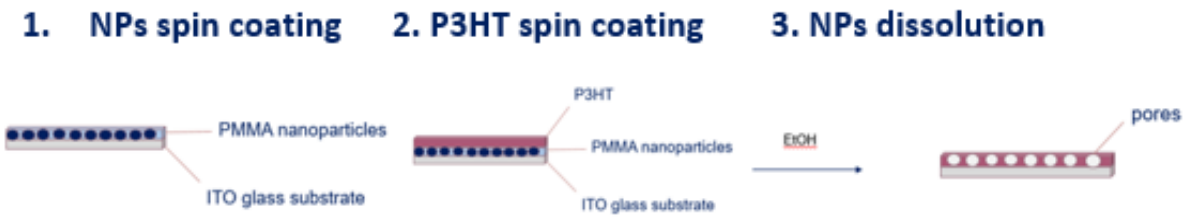

Figure 13. Schematic representation of the Nanoparticle Template Method.

2.4 Spin-Coating

Spin coating is a common technique aimed at the deposition of thin films on substrates. It consists of spinning a solution at high speeds using a device called spin coater. The combination of the *centripetal force* and the *surface tension* of the liquid creates an even covering. The key factor of this process is the *solvent evaporation*, which leads to the formation of a thin film in the range of a few nanometres to a few microns**.** [52–56]

Three phases can be identified in the process: (1) the *deposition*, (2) the *spin up* and (3) the *spin off*. The *deposition step* encompasses the casting of the solution onto the substrate surface. The amount of solution dropped depends on the *viscosity* of the fluid and the *size* of the substrate. Higher viscosity and larger substrates typically require larger amounts to ensure a full coverage. The deposition can occur in two ways: *Static* or *Dynamic.* While in the first case the casting occurs right before the spin coating starts the rotation, the Dynamic Spin Coating implies that the solution is cast on the substrate whilst spinning. The choice of the spin-coating mode depends mainly on the *type of polymer* and *solvent* used. Generally, the Dynamic Spin Coating is preferred when using rates higher than 1000 rpm as it becomes difficult to obtain complete substrate coverage with lower speeds. At spin rates lower than 1000 rpm, the static spin coating is preferred instead.

In the *spin up step*, the substrate accelerates to reach the desired rotational speed. In the meantime, an aggressive *fluid expulsion* occurs from the substrate due to the rotational motion. The fluid and the substrate spin at a *different rate*, creating a twisting effect, until eventually the rotation speed match up and the film becomes gradually thinner. Even though fluid thinning is usually *uniform*, when very volatile solvents are used, interference colours may appear as the solvent evaporates, gradually disappearing as the fluid gets thinner. Spin speeds for this stage range from 1500-6000 rpm, again depending on the fluid properties as well as the substrate. This step can take from 10 seconds to several minutes.

Finally, in the *spin-off step*, the film thickness is settled and the film dries completely, changing its colour. As the fluid continues to thin, the fluid stops flowing significantly. At this point, the evaporation of the volatile solvents becomes the main factor. As the solvents evaporate, the viscosity of the remaining solution increases, causing the fluid setting or solidification. [55,56]

Spin coating is a *simple*, *fast* and *low-cost* method. Its biggest advantage is the possibility to control the *film thickness*. The thickness is proportional to the inverse of the square root of the *angular speed* ($\mathbf{d \propto 1/\sqrt{\omega}}$), which means that the higher is the rotational speed, the thinner will be the film (Figure 14). Relatively minor variations of ± 50 rpm are sufficient to change the resulting thickness of the 10%.[55]

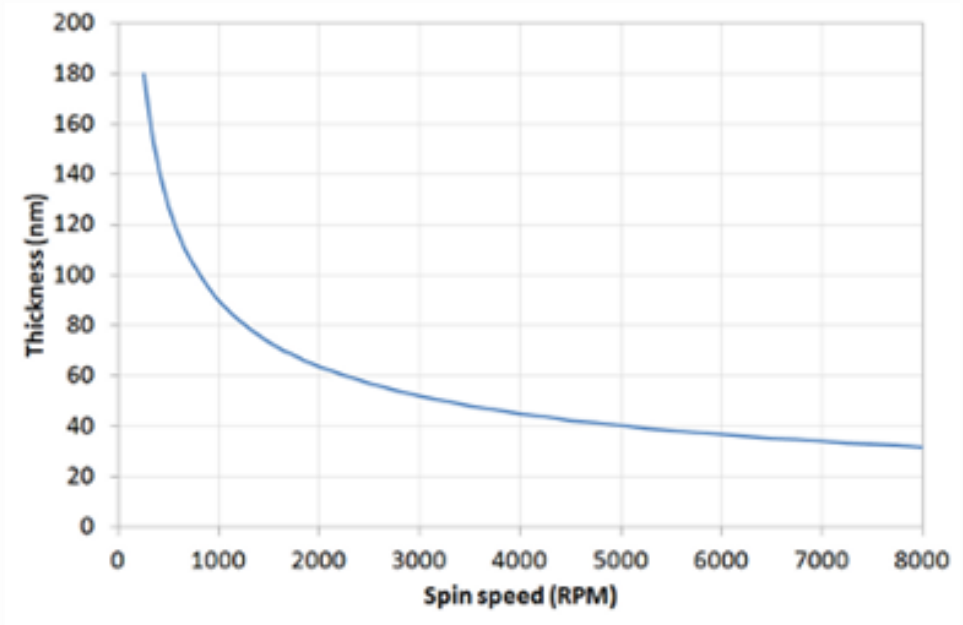

Figure 14. Dependence of the thickness to the spin speed. The curve reaches a plateau at high-speed rates (reproduced from: https://www.ossila.com/pages/spin-coating).

Additionally to the spin coating speed, other factors affect the final film thickness such as the *distance* of the substrate from the spin coater center, the *spinning time*, the *solvent volatility*, the *solution concentration* and the *interaction* between the polymeric chains. [56]

The use of an alternative spin coating technique, the *off-center spin coating*, represent a way to modify the film thickness. In contrast to the traditional method (on-center), in the off-center spin coating the substrate is placed at a distance (r) from the centre of the spin coater (Figure 15). The modification of this distance entails the film thickness modification. On the other hand, this method may also negatively affect the uniformity of the film thickness, with a thicker film at the edges. [57]

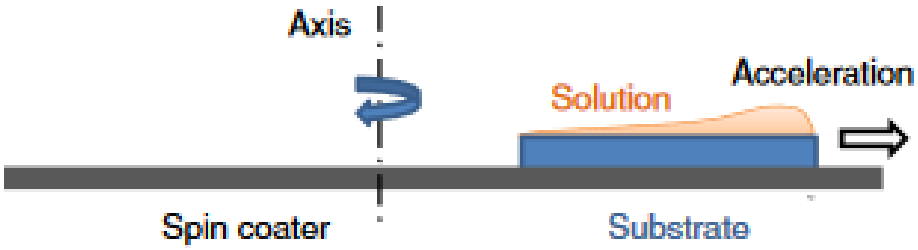

Figure 15. Thickness profile during off-center spin coating. (reproduced from: [51])

2.5 Vis-NIR absorbance Spectroelectrochemistry

The second objective of this work focuses on the study of the doping/dedoping kinetics of the p-P3HT films to establish the existence of a correlation between an ideally fast doping kinetic and the porous morphology of the film.

Steady-state Spectroelectrochemistry is an analytical technique that permits to obtain an electrochemical and spectroscopic response simultaneously. It consists of measuring the change in the absorbance spectrum of the studied material (P3HT in this case) when a V_{GS} voltage is applied to dope and dedope the film (oxidation and reduction of the polymer). [58,59]

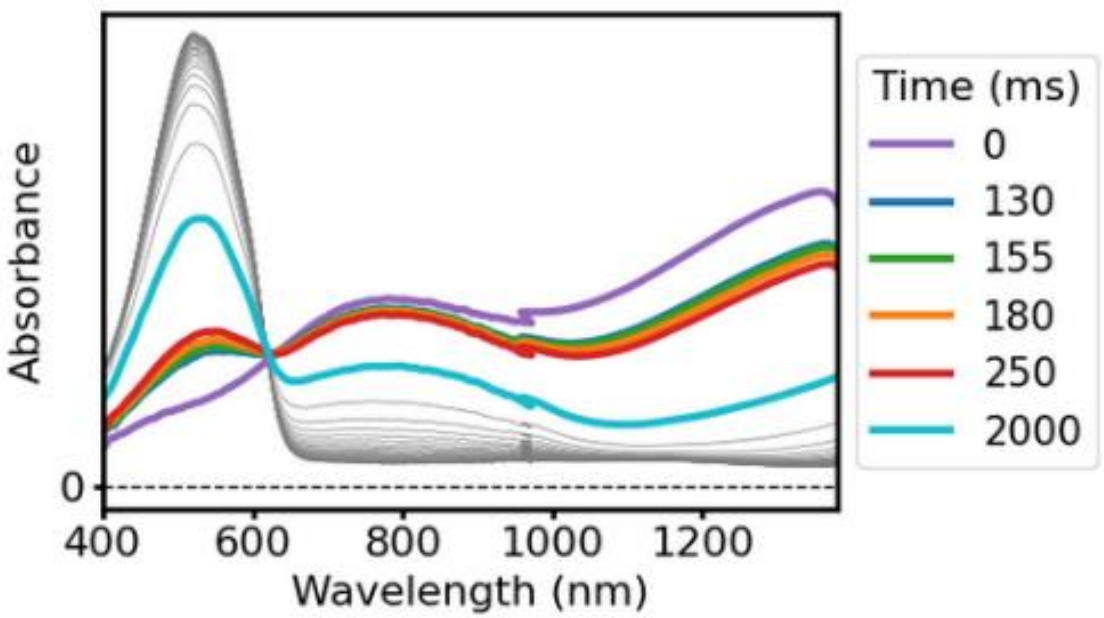

Figure 16. Steady State Spectroelectrochemistry absorption measurements p-P3HT, dwell (0N/OFF) = 60/60s, Vg (ON/OFF) = -0.8/0.4V.

Figure 16 is here used as reference example; it shows the typical behaviour of a P3HT film upon application of a dedoping V_{GS} voltage. For simplicity, the spectrum can be divided in three zones of wavelengths (λ) : (1) 400-600 nm (P3HT neutral domain), (2) 600-1000 nm, (3) λ > 1000 nm.

The film oxidation generates the decrease of the π-π* peak in zone 1 and the increase of the n-π* peak in zone 2, which represent a polaron species formation. A polaron is a quasiparticle representing an electron or hole coupled with the lattice distortion in a material, which forms

when the polymeric film oxidizes. As the gate voltage lowers down to the minimum doping value (-0,8V for P3HT), a bipolaron species forms, which causes the band increase in region 3. A bipolaron is a quasiparticle consisting of two bound polarons in a material. Finally, the signal at 900 nm is just noise due to the instrument; therefore, it does not give any information about the doping of the polymeric film.[33]

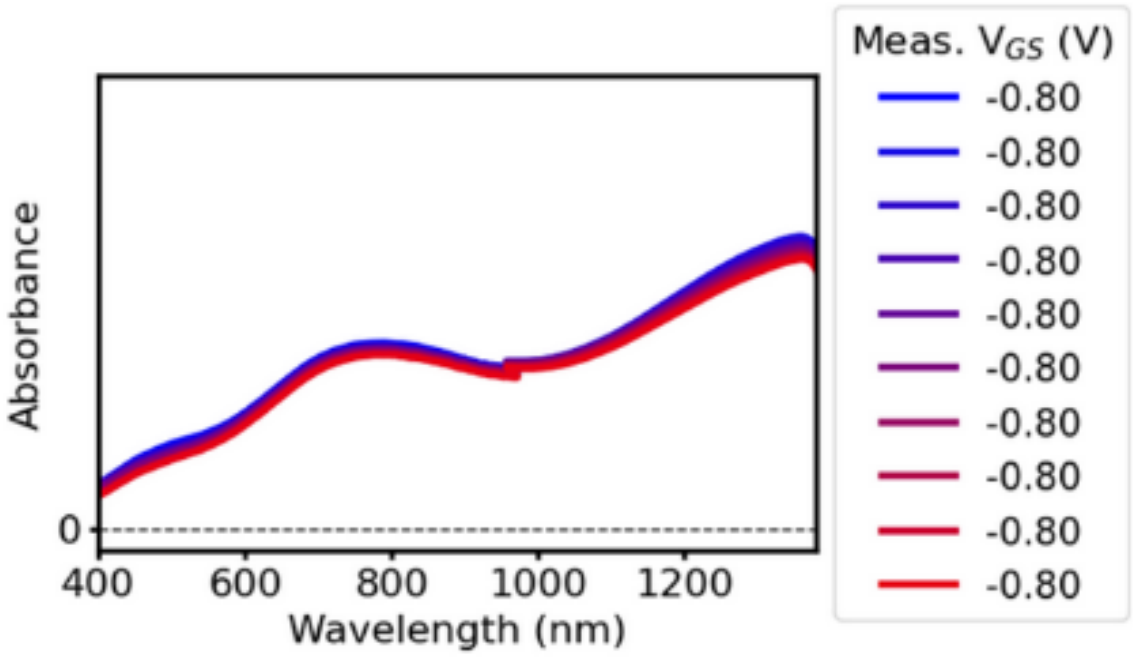

Figure 17. Steady State Spectroelectrochemistry absorption measurements p-P3HT at doping voltage (-0.8V).

The same analysis can provide additional information due to the possibility of performing the doping and the dedoping of the polymeric film multiple times, by selecting the number of cycles desired. As shown in Figure 17, if the absorbance spectra of the polymeric film at the doping voltage for each cycle overlay, it means that the sample has a *good doping stability*. This stability is further confirmed when plotting the Time vs. the Absorbance (Figure 18), which shows that the doping/dedoping state reach the same level for all cycles. Additionally, the *shape* of the curve in gives an idea of how fast the polymer dopes and dedopes (e.g. dedoping faster than the doping).

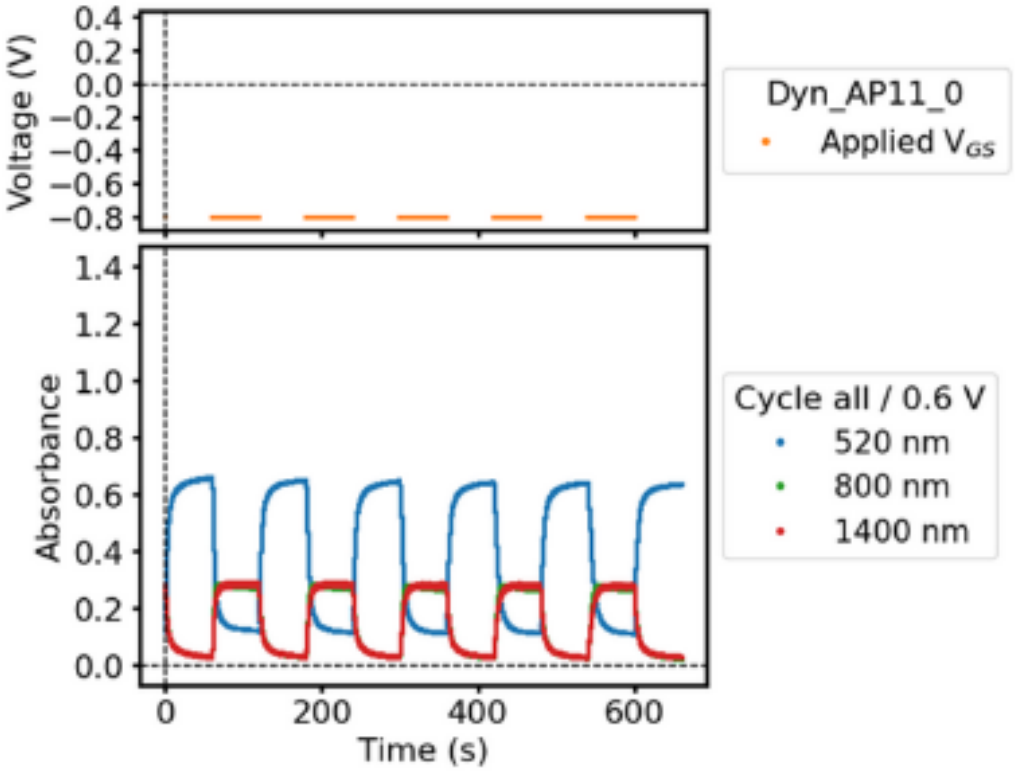

Figure 18. Time vs. Absorbance of p-P3HT.

In this study, all spectroelectrochemical measurements are taken in a *sandwich cell configuration* (Figure 19). In this setup, the voltage typically applied between the Source and Drain electrodes in a transistor configuration is replaced by the voltage between the conductive ITO glass substrate (acting as the working electrode) and the Ag/AgCl Gate electrode (acting as the counter electrode). When a negative voltage is applied to the gate electrode, anions from the electrolyte migrate into the active layer of the polymeric film (P3HT), which is oxidized. During the oxidation, charge carriers are injected into the polymer, enabling current flow through the polymeric film and the ITO substrate.

Simultaneously, the sample is irradiated with light, and the polymer absorbs part of this light, depending on its redox state. The intensity of the transmitted light is recorded by a photodetector, allowing for the generation of the polymer's absorbance spectra, which reflects changes in its electronic structure as a function of the applied potential.

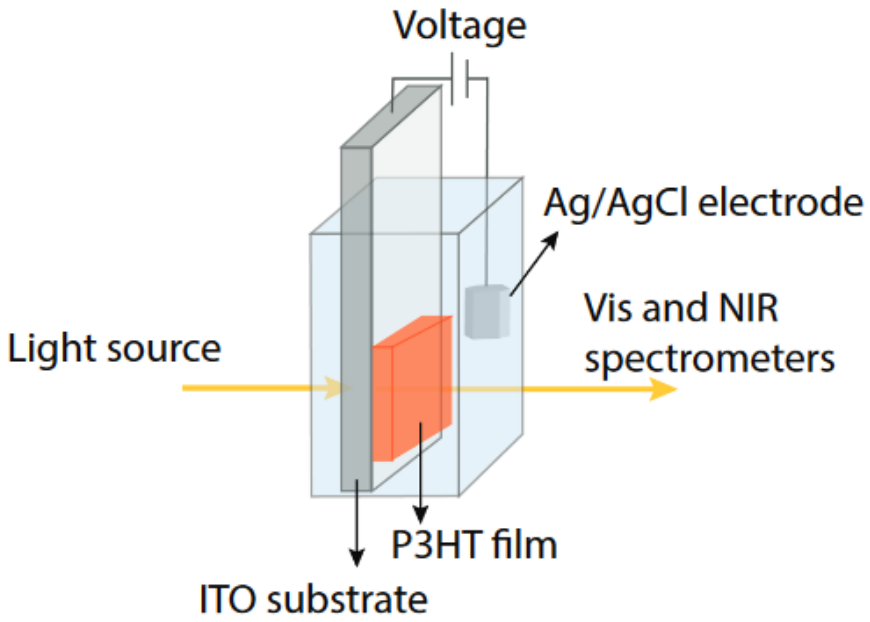

Figure 19. Experimental setup for the in situ Vis/NIR spectroelectrochemical measurements (reproduced from: [51]).

The Time Resolved Spectroelectrochemistry allows monitoring the temporal evolution of spectroscopic changes during an electrochemical reaction. In other words, it enables the observation of how the optical or electronic properties of the material change over time while the gate potential is applied. [58,59]

3. RESULTS AND DISCUSSION

In order to fabricate thin p-P3HT films, three different methods were explored: the *breath figure*, the *dry breath figure*, and the *nanoparticle template methods* (detailed in section

2. **METHODOLOGIES**). Among them, only the breath figure method, the most widely used one, proved successful.

In the case of the *dry breath figure* method, solutions of P3HT dissolved in chloroform ($CHCl_3$) with added water in the solutions were tested. Three chloroform solutions of P3HT at a fixed concentration of 5 mg/mL with varying water contents (1.5 wt%, 3 wt% and 5 wt% respectively) were spin coated (1^{st} step = 2000 rpm/2s; 2^{nd} step = 1500 rpm/90s) on an ITO glass substrate at ambient relative humidity (RH ~30%). The ITO substrates were cleaned before P3HT-coating by exposure to UV/O_3 for 5 minutes. Scanning electron microscope (SEM) analysis revealed **no pores in any of the three films**. Since this method has not been previously applied to P3HT, the exact reason for the lack of porosity remains unclear. Probably, the absence of pores resulted from a combination of the *low polymer concentration*, the *low water content*, and particularly the use of chloroform, a *water-immiscible solvent*, which may have been unsuitable for this technique.[50] If given more time, based on the observations from this preliminary test, the next experiment would have been to test the effect of different concentrations, water amounts and solvents to optimize the parameters controlling the dry breath figure success.

In the case of the *nanoparticles sacrificial template* method, PMMA nanoparticles (diameter of 100 nm) were spin-coated onto an ITO substrate (cleaned in the UV/O_3 cleaner for 5 min). This was followed by spin-coating a 15 mg/mL P3HT solution in o-xylene (which is a good solvent for PMMA and bad solvent for P3HT) (see section 2.3) using a two-step process (1^{st} step: 2000 rpm/2 seconds; 2^{nd} step: 1500 rpm/90 seconds). The resulting film was then immersed in an ethanol bath for 3 hours to dissolve the PMMA nanoparticles without affecting the P3HT film.

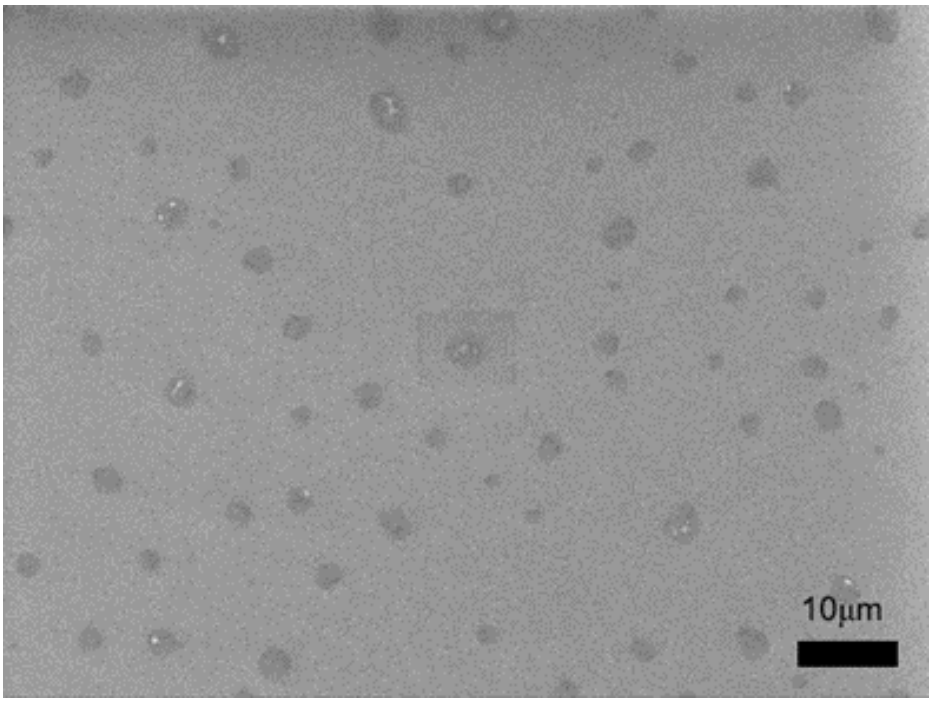

Figure 20. SEM image of PMMA nanoparticles spin-coated on an ITO substrate at 200 rpm/60s after three consecutive casting

The primary challenge with this method is to determine the optimal spin-coating speed for the nanoparticle layer. Despite some articles suggesting the use of high spin-coating speeds[52,60,61], when the PMMA nanoparticle solution was spin-coated at 3000 rpm/60s (repeated three times), SEM analysis revealed no particles on the sample. Reducing the speed to 200 rpm/60s proved slightly more effective, as shown by the presence of nanoparticles observed by SEM (Figure 20). However, nanoparticle deposition remained too inhomogeneous, with particles primarily found at the edges of the sample and lacking uniformity in size. Besides, after completing the procedure, as described above, the resulting P3HT film appeared dense, with no noticeable porosity (Figure 21).

Given that the goal is to achieve *reproducible* porous P3HT films with *full pore coverage* and pore sizes in the range of 200 nm to 800 nm these two methods were set aside as more promising results found during the preliminary tests made using the *breath figure* method. The results achieved by this latter method are presented in detail below.

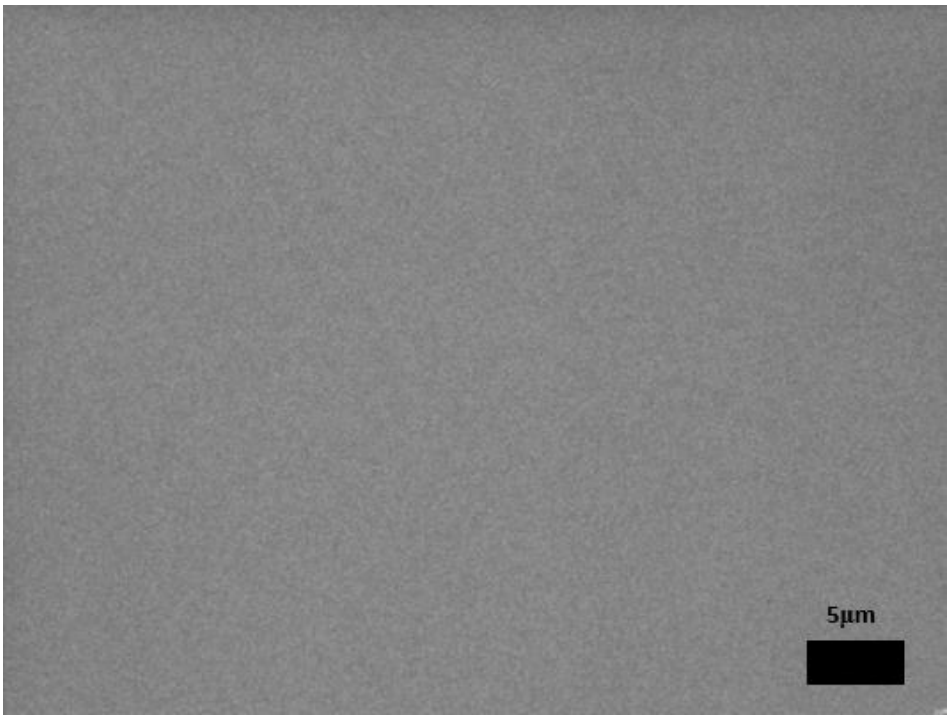

Figure 21. SEM image of P3HT after ethanol bath.

3.1 P3HT porous films

To determine the optimal parameters for achieving porosity using the *breath figure* (BF) method, we made the hypothesis that the five following variables affect the film porosity: *P3HT/SEBS ratio*, s*olvent*, *concentration*, r*elative humidity (RH), spin-coating method.* The impact of each variable was then quantified in systematic studies by changing one parameter only while keeping the five others constant.

3.1.1 Spin coating speed

Although the spin coating speed is an important factor influencing the formation of porous films, no specific experiments were taken to determine the optimal speed. Instead, the selected values were based on theoretical considerations, which appear to fit well with the observed experimental results.

In general, the spinning time needs to be long enough for the solvent to fully evaporate and for the film to dry on the substrate (at least 30 seconds when using chloroform). When applying spin-coating in the Breath Figure method, the speed and duration should be carefully selected, as they affect the rate at which water droplets form and enter the solution, thus affecting how droplets arrange, which determines the final porosity of the film. Additionally, the speed indirectly influences porosity by altering the film thickness. [45,62]

In light of all these considerations, the speed chosen was:

- **2000 rpm/2s** (first step), which determines the *thickness* and give sufficient time for the fluid to dry over the majority of the substrate;
- **1500 rpm/90s** (second step), which removes excess solution from the corners and dries the rest of the substrate. The spin coating duration is higher than the one mentioned above, because of the humid environment, which slows down the drying process.

3.1.2 P3HT/SEBS ratio

As previously mentioned, the BF method was the only approach that enabled the formation of porous films. Based on its use in literature,[63,64]Styrene-Ethylene-Butylene-Styrene (SEBS) was used as an additive (Figure 22). It is still not completely clear how SEBS affects the final morphology of the film, but it is known that SEBS is a *thermoplastic elastomer* with *good mechanical* and *electrical properties*. Hence, its use may be to benefit from its *good flexibility* (in view of a possible bioelectronics application) and its ability to soften organic semiconductor films, such as P3HT, leading to scalable transfer process.[63,64]

To investigate the effect of different P3HT/SEBS ratios, four solutions were prepared: pure P3HT in 100% chloroform (for reference), *vs.* P3HT/SEBS (1:1 wt%), P3HT/SEBS (2:1 wt%) and P3HT/SEBS (3:1 wt%) in a chloroform/methanol solvent mixture (92:8 vol%). All solutions were prepared at the same concentration (6 mg/mL) and spin-coated onto ITO glass substrates, which were cleaned in a UV/O_3 cleaner for 5 minutes. The spin-coating process was conducted under identical conditions: room temperature, 90% relative humidity and a two-step spin coating of 2000 rpm/2s (1^{st} step) and 1500 rpm/ 90 s (2^{nd} step).

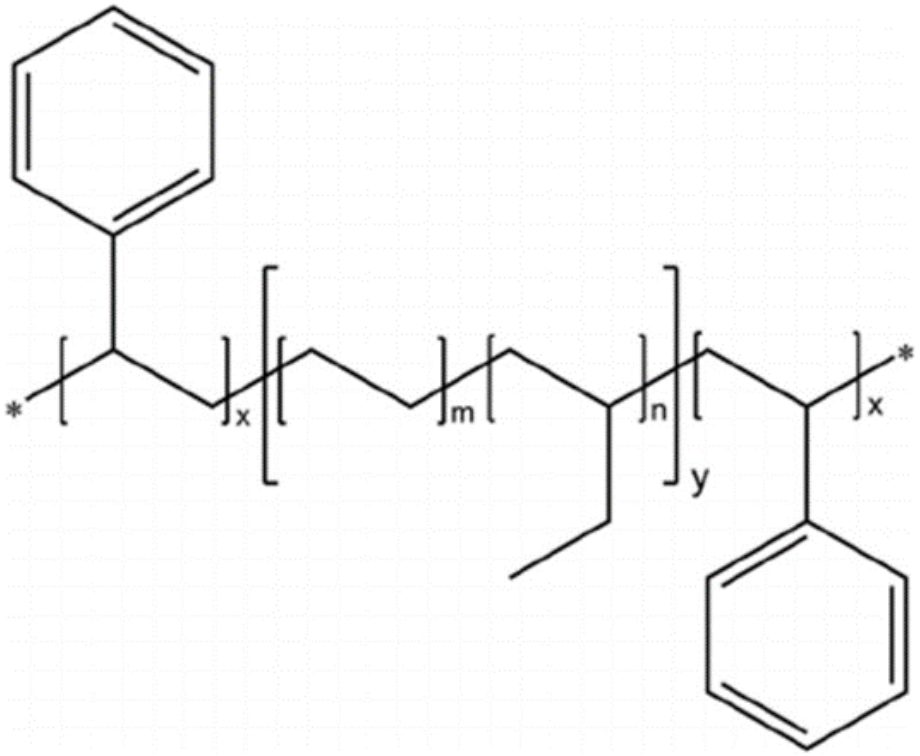

Figure 22. Chemical structure of Styrene-Ethylene-Butylene- Styrene (SEBS).

SEM images show no obvious pores in the reference film prepared without SEBS. Similarly, the films prepared with a 1:1 wt% ratio and 3:1 wt% ratio show no clear evidence of pores. On the other hand, the film prepared with a P3HT/SEBS 2:1 wt% ratio is successfully porous, displaying in pores of diameters ranging from 380 nm to 650 nm (Figure 23). However, no full film pore coverage and no film homogeneity was achieved, thereby encouraging optimizing the other five parameters.

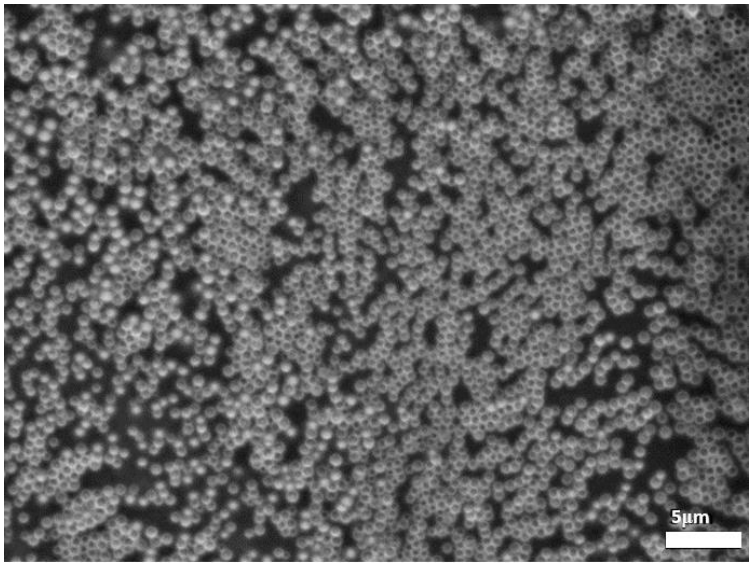

Figure 23. SEM image of a P3HT/SEBS film prepare with a 2:1

In summary, using a solution with P3HT/SEBS ratio of 2:1 seems to be more suitable to prepare porous P3HT films rather than no additive and different ratios.

3.1.3 Solvent

The second hypothesis focuses on the influence of the organic solvent on the film porosity. Two primary factors have driven the solvent selection: i) the Breath Figure method requires a *highly volatile* solvent with a boiling point (T_b) below 100 °C to ensure its evaporation *before water*, ii) the solvent must dissolve both P3HT and SEBS effectively, while being miscible with water. The solvents listed in the Table 2 below satisfy these criteria. Among these, chloroform is the most widely used in the literature.[65–67]

Solvent	**P3HT solubility (mg/mL)**	**Miscibility with H_2O (mg/mL)**	**T_b (°C)**
Chloroform	>10	8	61
Trichloroethylene	>10	1.1	87
Thiophene	4-6	0.003	84

Table 2

Some articles also report the use of a small percentage of methanol (CH_3OH) to improve the uniformity of porous films, despite the poor solubility of P3HT in it.

Four solutions of P3HT/SEBS (2:1) with a fixed concentration of 15 mg/mL were prepared in **different solvents:** *Chloroform, Chloroform:Methanol mixture* (92:8 vol%), *Trichloroethylene* and *Thiophene*. Each solution was spin-coated onto an ITO substrate at the same conditions, that is room temperature, a relative humidity of 90% and spin coating speed of 2000 rpm/2s (1st step) and 1500 rpm/ 90 s (2nd step).

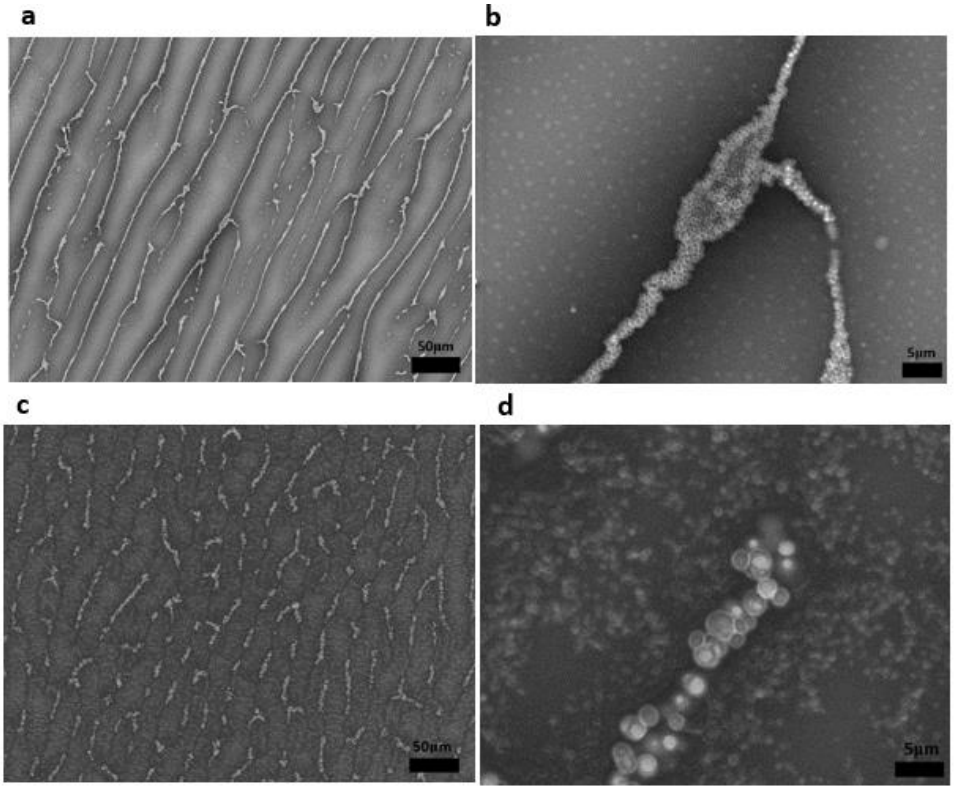

Figure 24. SEM images of the P3HT/SEBS (2:1) at RH= 90% in a-b) CHCl3; c-d) CHCl3/CH3OH.

SEM images reveal pores only in films prepared in Chloroform and Chloroform:Methanol mixture. The diameter of the observed pores are ranging from 120 nm to 950 nm and 600 nm to 3000 nm, respectively (Figure 24**Errore. L'origine riferimento non è stata trovata.**). The addition of methanol resulted in larger pores but a more controlled and regular pore distribution as well as a more homogeneous film overall. This is in accordance with literature in which this

is attributed to the property of methanol to favor the evaporation process of the organic solvent and minimize the heat capacity of the substrate.[64]

The lack of porosity in films prepared using thiophene and trichloroethylene can probably be attributed to their higher boiling points (84 °C and 87 °C), compared to chloroform (61 °C), which interfere with the Breath Figure process.

In summary, the solvent choice is crucial not only for the achievement of porosity, but also for the control of the pore size.

3.1.4 Concentration of P3HT/SEBS blend solutions

As already mentioned in 2.1.4 Concentration, higher the concentration of the polymer is, slower the solvent evaporation will be, higher the number of condensed water droplet forming (creating a stacking of water droplets) will be, and consequently higher the number of pores and larger their size will be.[51,68,69]
To investigate the effect of solution concentration on porosity (size, morphology, distribution across the film), four P3HT:SEBS (2:1 wt%) solutions were prepared under the same conditions of the previous experiment, meaning using a chloroform/methanol (92:8 vol%) solvent mixture, but **varying the concentrations** as follow: 4 mg/mL, 6 mg/mL, 10 mg/mL, 15 mg/mL.

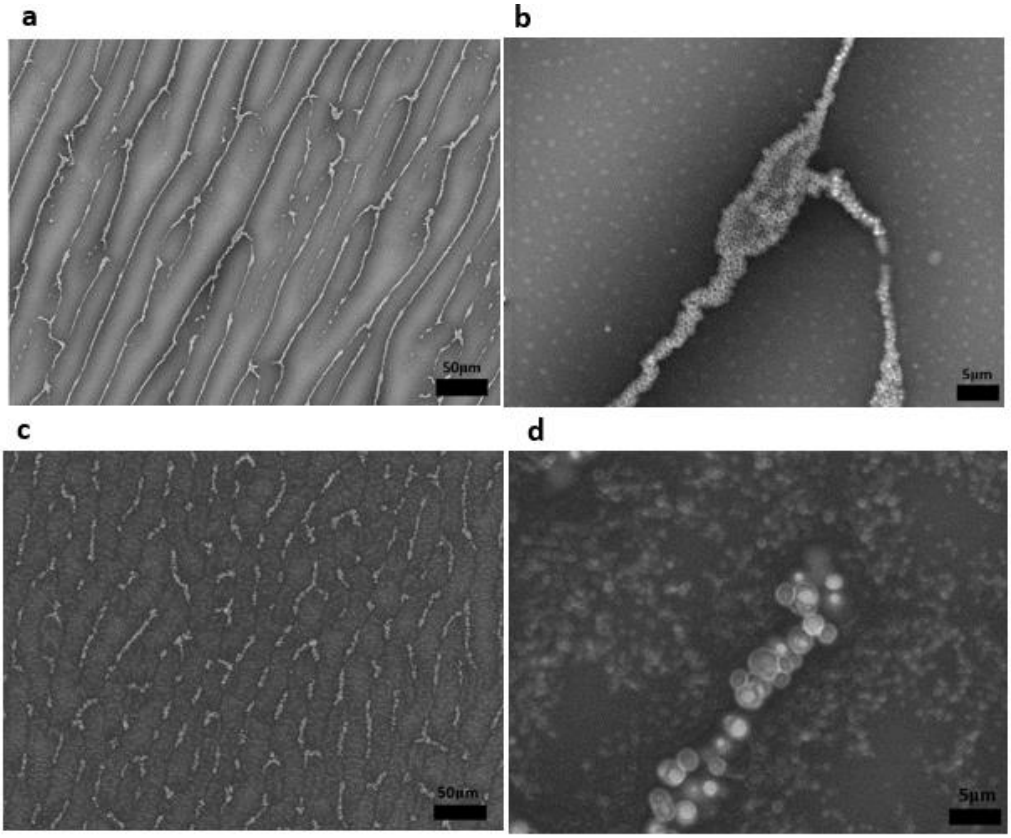

Figure 25. SEM images of the P3HT/SEBS (2:1) at RH= 90% in a-b) $CHCl_3$; c-d) $CHCl_3/CH_3OH$.

SEM images show a lack of porosity in the film with the lowest concentrations (4 and 6 mg/mL) and an increasing coverage across the film as the concentration increases (Figure 25). However, even in this case, complete pore coverage of the film was not achieved. This result can be explained considering that a low concentration of the polymer mixture can cause the coalescence and disruption of the water droplet array, due to the insufficient solute to stabilize the droplets.[42,47]

As shown in Figure 26, the pore arrangement in the film varies depending on the concentration of the P3HT/SEBS blend solution. The sample with the highest concentration (15 mg/mL) exhibit a more uniform pore distribution and arrangement (Figure 26 c-d). However, unexpectedly, no significant difference was found in the pore size, exhibiting round shapes with diameters of 200-1800 nm for all films casted from both 10 mg/mL and 15 mg/mL solutions.

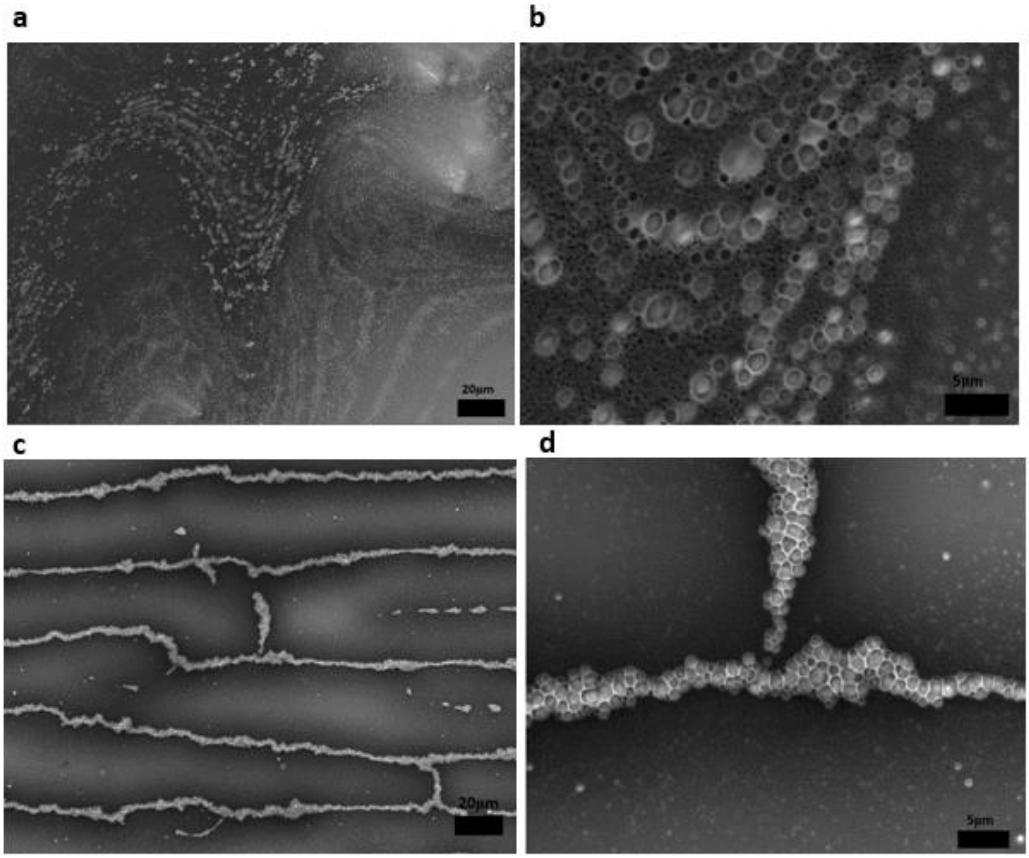

Figure 26. SEM images of the P3HT/SEBS (2:1) in $CHCl_3/CH_3OH$, RH=90%, at a-b) 10 mg/mL, c-d) 15 mg/mL.

3.1.5 Relative humidity

Relative humidity (RH %) plays a crucial role in the Breath Figure method. Values above 60% are required for the process to be effective.[45] As the relative humidity increases, water droplets grow faster, allowing control over the number and size of the pores. The aim is to maintain a constant temperature (~25°C) and minimize any fluctuations during the Breath Figure process, so that the effect of relative humidity on porosity can be isolated.

A new set of P3HT (10 mg/mL) thin films was prepared under the same conditions as previous experiments, with **varying relative humidity** of 60%, 70%, 80%, and 90% for each sample. SEM analysis confirmed that higher RH% increases porosity, resulting in greater pore coverage (though not complete) and a slightly more regular morphology, characterized by lines of pores. Specifically, films prepared at 60% and 70% RH were found to be non-porous, while those at 80% and 90% RH exhibited porosity (Figure 27). However, unexpectedly, no significant differences in pore size were observed, with diameters ranging from 200 nm to 2000 nm.

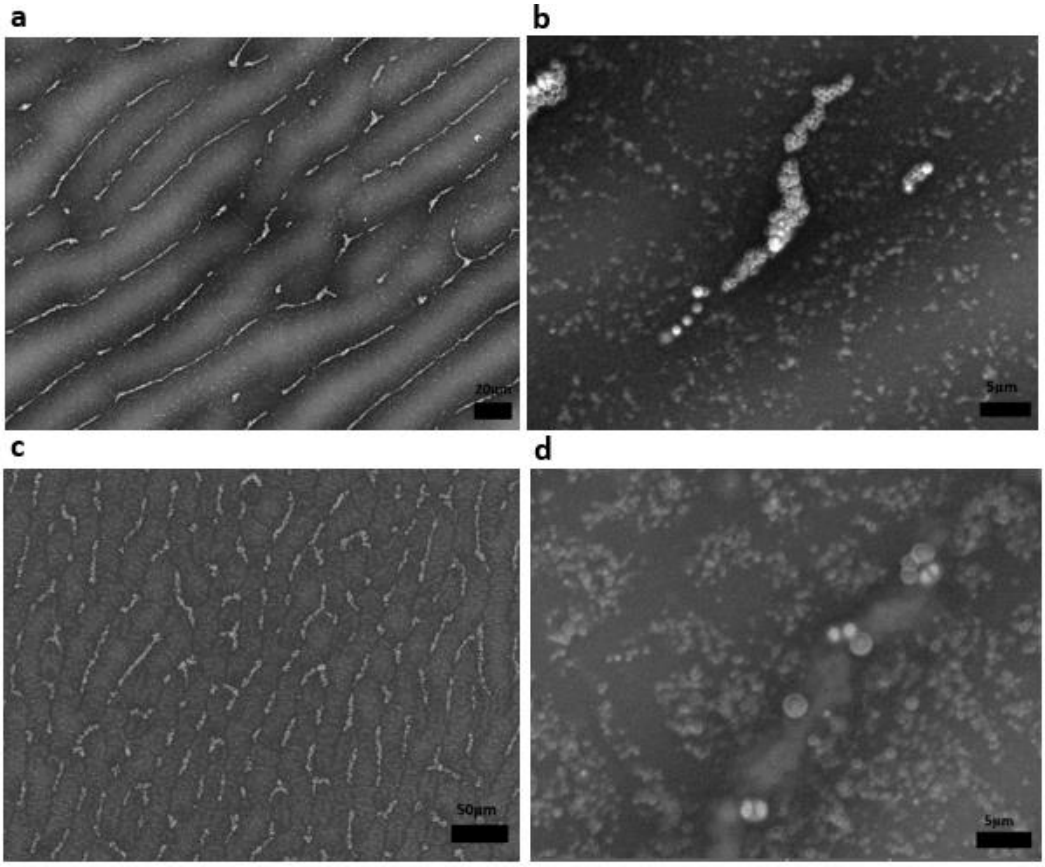

Figure 27. SEM images of the P3HT/SEBS (2:1) in $CHCl_3$/CH_3OH at 10 mg/mL a-b) RH=80% c-d) RH=90%.

3.1.6 Spin-Coating Method

The final parameter influencing porosity is the spin-coating method itself. In all previous experiments aimed at optimizing porosity, the *dynamic **on-center** spin coating* method was used due to its ability to spread the polymer across the entire surface of the substrate. However, this method did not result in full *pore coverage* across the film. Even after optimizing humidity, concentration, and organic solvent, pores were only observed at the edges, leaving the central area of the film uncovered. By switching from on-center to **off-center** spin-coating, greater pore coverage is achieved (see section 2.4 Spin-Coating). Off-center spin-coating involves placing the substrate at a distance from the center of rotation, which allows better control over film *thickness* and, as seen below, porosity.[62]

Several films of P3HT and P3HT/SEBS (2:1) were prepared using the off-center spin-coating method with two different solvents: pure chloroform and a chloroform/methanol mixture (92:8 vol%). The experimental setup involved a polymer concentration of 15 mg/mL and spin-coating at room temperature. The process included two steps spin coating, 2000 rpm/2s for the first step and 1500 rpm/90s for the second step. The films were coated onto ITO substrates, pre-cleaned for 30 minutes in a UV/O_3 cleaner. The experiments were conducted at 80% and 90% relative humidity, as both outputted promising results as shown above .

SEM images reveal **porosity in all samples**. In particular, the combination of (i) pure P3HT, (ii) off-centre spin-coating, (iii) chloroform/methanol mixture solvent, and (iv) an 90% RH is the best parameters to achieve our objectives. Indeed, the resulting films exhibit a higher pore coverage, **solving the problem of lack of porosity in the center of the film,** and allowing to achieve the **desired pore size**, with a diameter ranging from 200 to 880 nm (Figure 28a-d).
These experiments proved that promising results could also be achieved without SEBS as additive. Nonetheless, its use is still encouraged since it enhances the film pore coverage.

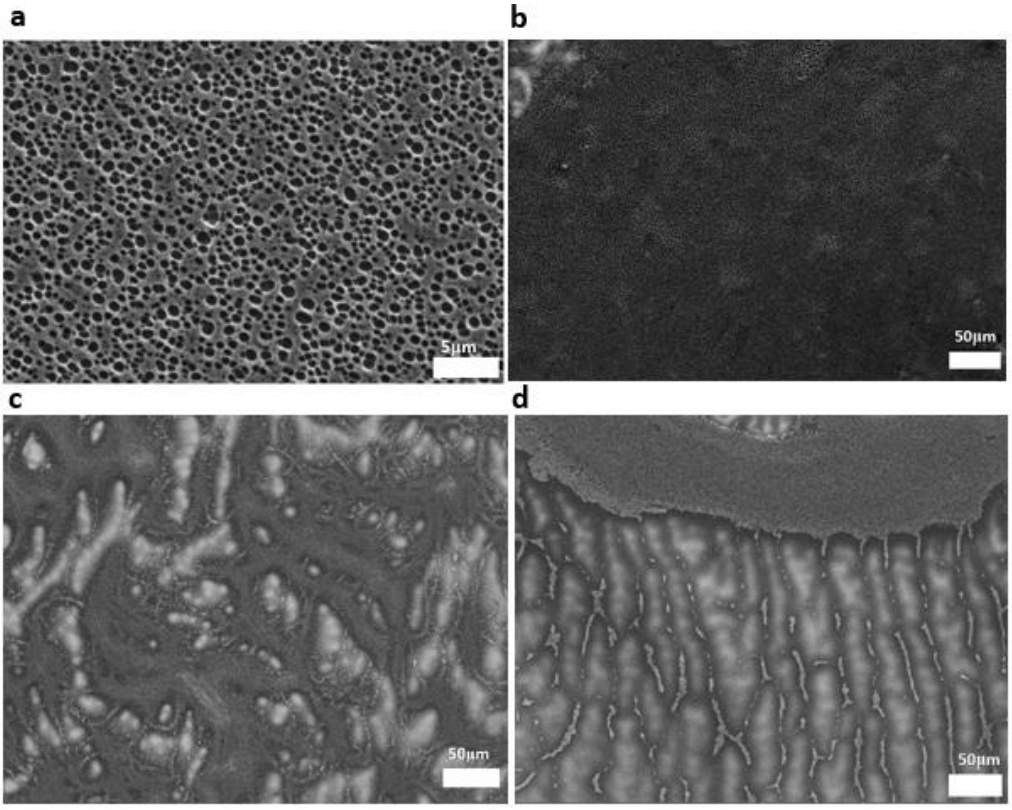

Figure 28. SEM images casted from in $CHCl_3/CH_3OH$ (92:8 vol%) solutions of a-d) pure P3HT RH=80%); b-c) P3HT/SEBS 2:1 RH= 90%.

The pore morphology varies across the different films when varying pure P3HT vs. P3HT/SEBS (2:1) and 80% vs. 90% RH (Figure 28) and is not completely homogeneous. The film prepared with only P3HT in pure chloroform shows pores mainly arranged in lines (Figure 29a). However, when SEBS is added, the film exhibits a honeycomb structure at the edges and a line arrangement toward the center (Figure 29b-c). In contrast, changing the solvent to a chloroform/methanol mixture, for the film prepared with P3HT/SEBS at 90% RH, results in a nearly complete honeycomb pore structure covering almost the entire surface (Figure 28 b-c). While the pure P3HT film, using the same solvent mixture, results in a film displaying mainly a honeycomb pore structure, with some areas still showing line organization (Figure 28d).

In summary, **the preparation of porous P3HT film (p-P3HT) is successfully achieved by using breath figure technique**. In addition, controlling parameters such as relative humidity, solvent, concentration, and spin coating speed improves pore coverage, achieving pore sizes of 200-880 nm. Optimal conditions included 90% RH, a 92:8 Chloroform:Methanol mixture, a two-step spin coating (2000 rpm for 2 s, 1500 rpm for 90 s), and off-center spin coating method.

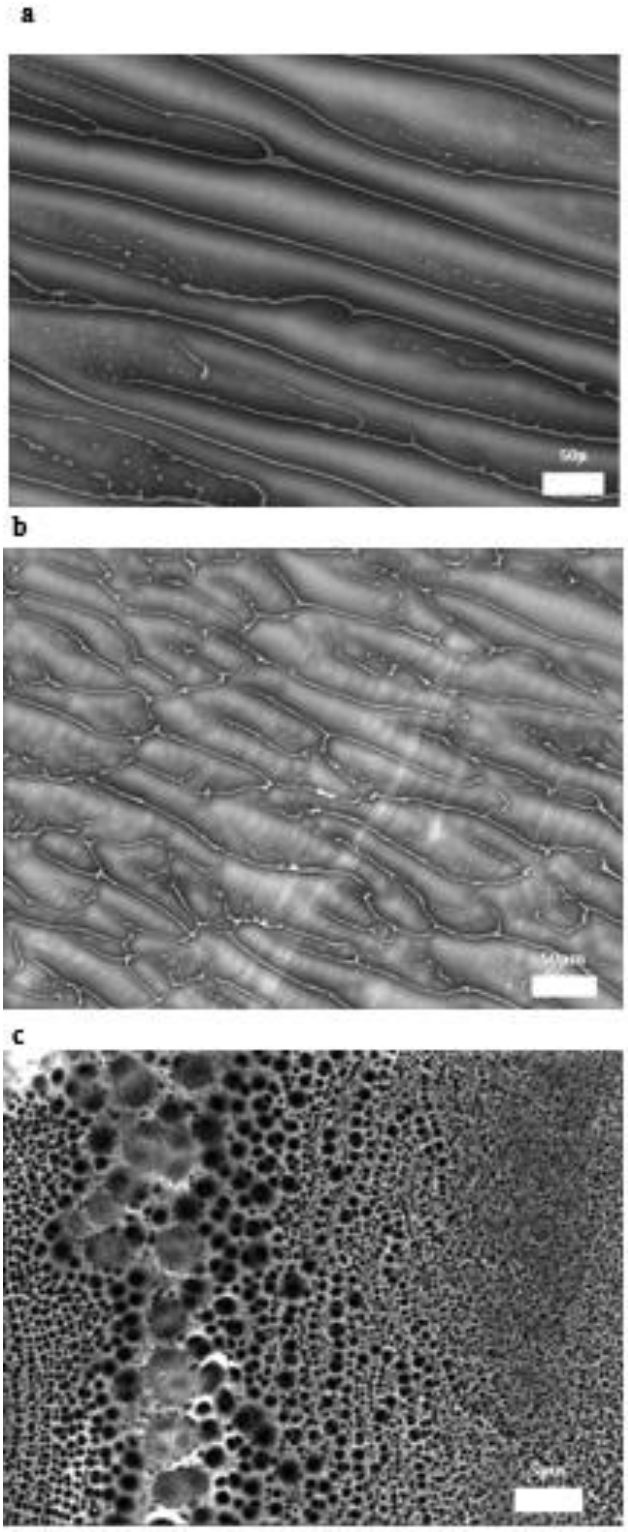

Figure 29. SEM images casted in $CHCl_3$ solution of a) pure P3HT RH=90%); b-c) P3HT/SEBS 2:1 RH= 90%.

3.2 Kinetic Performance of porous P3HT films

In this section, the influence of P3HT polymer film morphology on doping kinetics is examined. More specifically, the doping kinetics of p-P3HT and d-P3HT are compared to verify the hypothesis that the introduction of pores enhances the doping kinetic process. [39] For this reason, the most porous samples are selected for time-resolved Vis-NIR absorbance spectroelectrochemical analysis. In particular, we will evaluate how the following factors affect the kinetics: *SEBS presence*, *spin-coating method*, *crystallinity* and *pore arrangement*.

Before discussing the obtained results, it is essential to underline that, additionally to the morphology of the polymer used as the channel in an OECT, doping kinetics also depend on *ionic mobility* (see 1.2.2 Kinetic performance). Hence, the choice of electrolyte plays a critical role. Faster doping rates are achieved with *large, minimally hydrated*, and *highly polarizable ions* due to their *lower doping activation energy*.[28,39] For this reason, 0.1 mol L^{-1} *aqueous potassium hexafluorophosphate* **(KPF_6)** electrolyte, which satisfies these criteria (see Table 3), was selected for all measurements. Moreover, given that this is an aqueous electrolyte, the applied voltage for doping and dedoping cycles of the semiconducting polymer must remain within the *electrochemical stability window* of water. [34] Therefore, a gate voltage of -0.8 V was applied to dope P3HT films, while +0.4 V was applied to dedope them.

Anion	Ionic Radius (Å)	Anhydrous Volume* ($Å^3$)	Hydration # in bulk water	Polarizability α_0 ($Å^3$)
F^-	1.26[1]	8.4	6.7[2]	1.144[3]
Cl^-	1.68[1]	19.9	6.4[2]	3.253[3]
Br^-	1.90[1]	28.7	5.9[2]	4.748[3]
ClO_4^-	2.25[1]	47.7	3.8,[4] 4.6[5]	4.825[3]
PF_6^-	2.52[1]	68.6	1.7[6]	
$TFSI^-$	3.27[7]	146.5	~0[8,9]	6.402[3]**

Table 3. Anion properties; as a general trend the larger ionic radius and greater the polarizability result in lower hydration numbers. (reproduced from: [19])

As observed in the previous section, the addition of SEBS increases the pore coverage of the P3HT film. Therefore, when comparing a p-P3HT with a p-P3HT/SEBS one, it would be expected that the most porous sample (with SEBS) would exhibit faster doping kinetics. Moreover, both porous samples would be expected to show faster doping rates than their dense

counterparts (d-P3HT). However, *time-resolved spectroelectrochemistry* reveals that the most porous sample, p-P3HT/SEBS (red), not only exhibits slower doping kinetics than d-P3HT/SEBS (blue), but is also slower than p-P3HT, the porous sample without the additive (Figure 30). Moreover, the doping kinetics of d-P3HT and d-P3HT/SEBS are nearly identical, as are those of p-P3HT (yellow). This discrepancy could be partly attributed to the differences in film thickness. The d-P3HT/SEBS film has a thickness of 578 mOD, while the d-P3HT film is thicker at 1000 mOD. Similarly, the p-P3HT film is thicker (1144 mOD) compared to the p-P3HT/SEBS film (949 mOD). Since thicker films can slow down ion transport during the doping process, the thicker porous samples may exhibit slower kinetics despite their higher surface area. This could explain why the expected trend in doping kinetics is not observed.

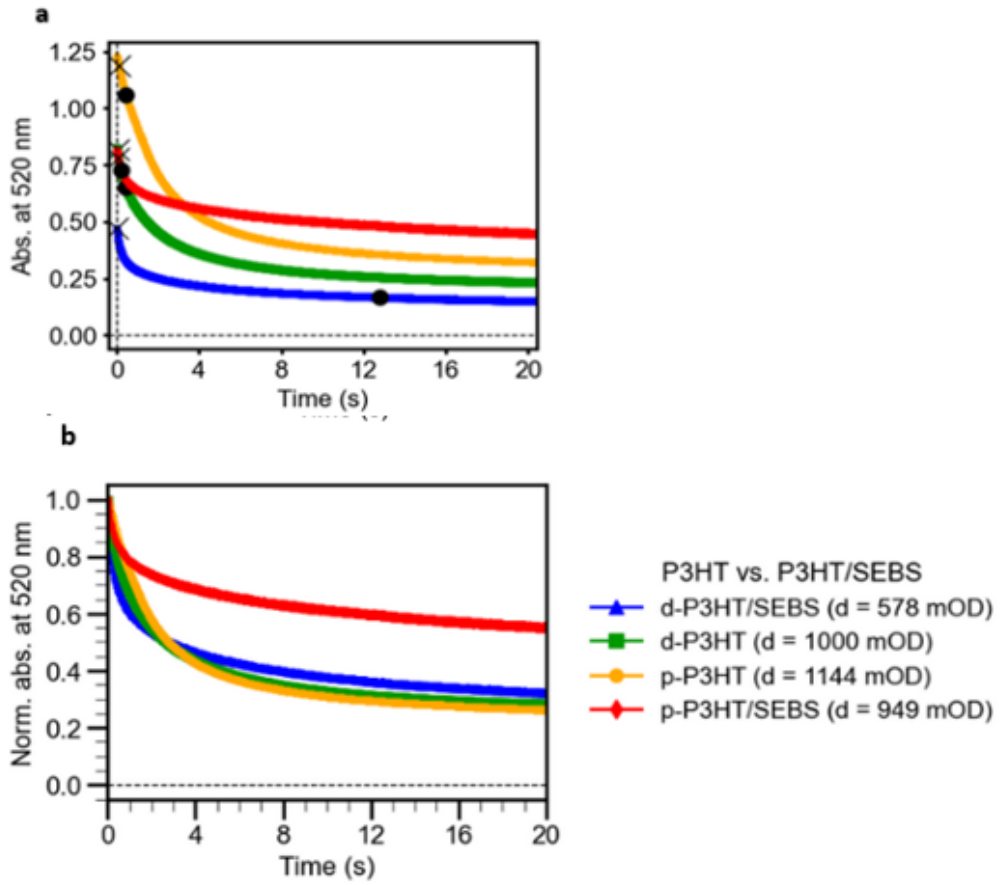

Figure 30. Temporal evolution of the absorbance at 520 nm (neutral peak of P3HT, wavelength sampling) upon P3HT doping at -0.8 V. a) raw data, b) normalized data of p-P3HT, d-P3HT, p-P3HT/SEBS (2:1), d-P3HT/SEBS (2:1).

Figure 31 shows two samples prepared under identical conditions but with different spin-coating methods, *on-center* and *off-center* respectively, which are compared to the corresponding dense film. While the porous films exhibit slower doping kinetics than the dense film (in blue), the off-center spin-coated film (yellow), with greater pore coverage, shows faster kinetics than the on-center film (green). At first glance, this aligns with the hypothesis that higher pore coverage should lead to faster doping kinetics. However, it is important to note that the films have different thicknesses: 578 mOD for the dense film, 1040 mOD for the on-center film, and 949 mOD for the off-center film. Given that the faster doping kinetics are observed in the thinnest film (578 mOD), the difference in thickness is likely a key factor driving the observed kinetics. Thinner films generally allow for faster ion transport, which could explain why the dense film dopes faster despite having lower pore coverage. Thus, while pore coverage may contribute, the variation in film thickness makes it difficult to conclusively attribute the results to porosity alone.

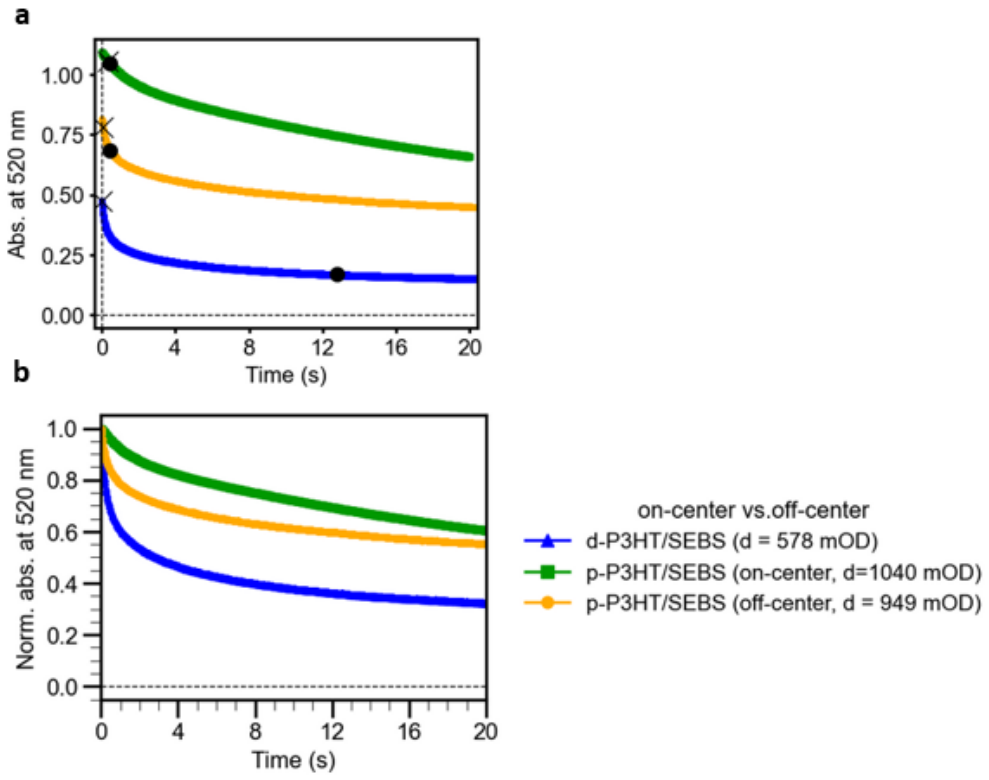

Figure 31. Temporal evolution of the absorbance at 520 nm (neutral peak of P3HT, wavelength sampling) upon P3HT doping at -0.8 V. a) raw data, b) normalized data of d-P3HT/SEBS, p-P3HT/SEBS (on-center), p-P3HT/SEBS (off-center).

Another key factor influencing the different doping rates is that off-center spin coating enhances film crystallinity, thereby increasing *electron mobility* and subsequently improving doping kinetics. [33,57,62] This is confirmed by the Vis-NIR absorbance spectra of the two porous films (Figure 32). The off-center spin-coated sample (more porous and faster) shows three peaks in its neutral state around 520 nm, 540 nm, and 600 nm, indicating a crystalline structure not observed in the more amorphous on-center sample.[71]

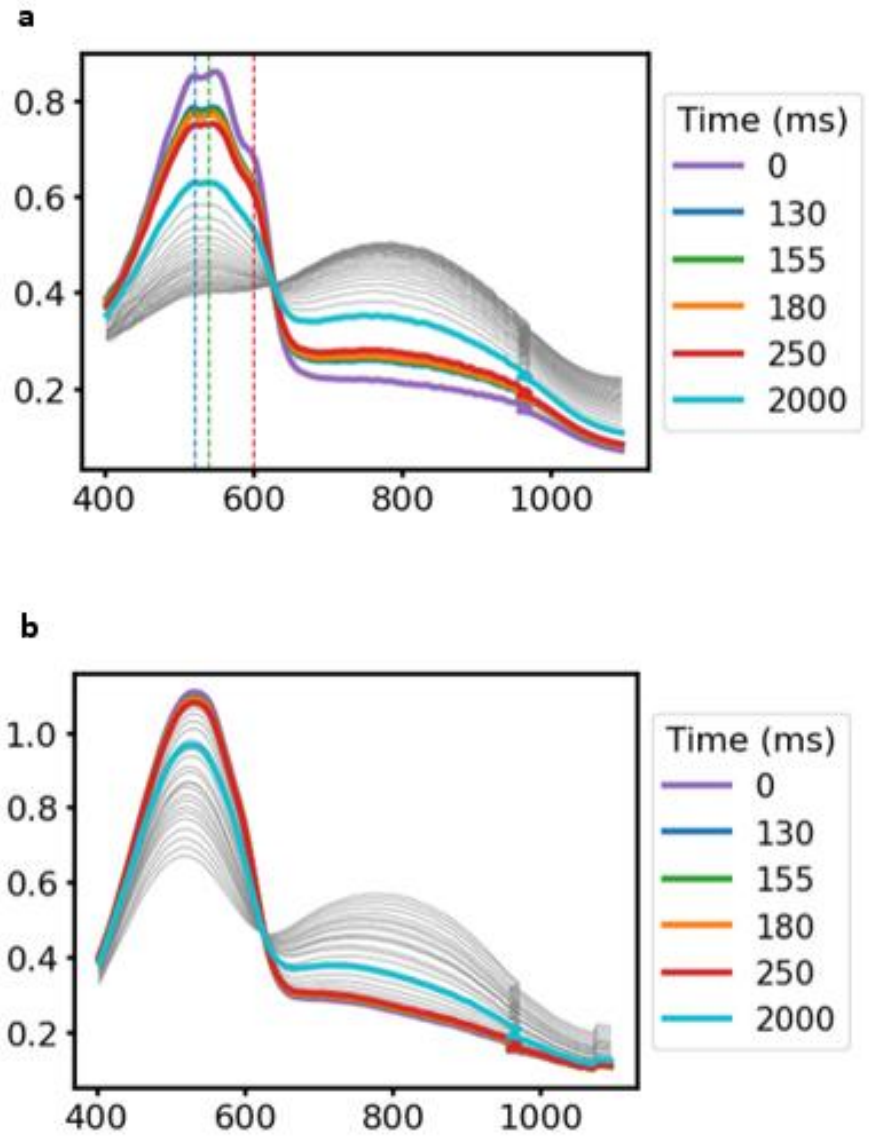

Figure 32. Evolution over time of Vis-NIR absorbance spectra upon P3HT doping at -0.8 V. of a) P3HT/SEBS (2:1) prepared by off-center spin coating and b) P3HT/SEBS (2:1) prepared by on-center spin coating; Vg ON/OFF= -0.8/0.4 V, steps=0.1V, 10 cycles.

Finally, p-P3HT films with different pore arrangements, one with a *honeycomb structure* and the other with *linear pores*, are compared. Figure 33 shows that films with a pore line arrangement (yellow) displays a significantly faster doping kinetic compared to the film with the honeycomb pore arrangement (green). Here, the thickness of the 'lines' sample is larger than the thickness of the 'honeycomb' sample and it is yet still faster. We can therefore conclude that **the line pore arrangement is actually a satisfying structure to accelerate doping of P3HT film**. Note that the p-P3HT with the linear pore arrangement and the d-P3HT have very similar doping kinetic rates, but the d-P3HT film is significantly less thick (about 2 times thinner according to the raw absorbance data) no relevant conclusion can be made.

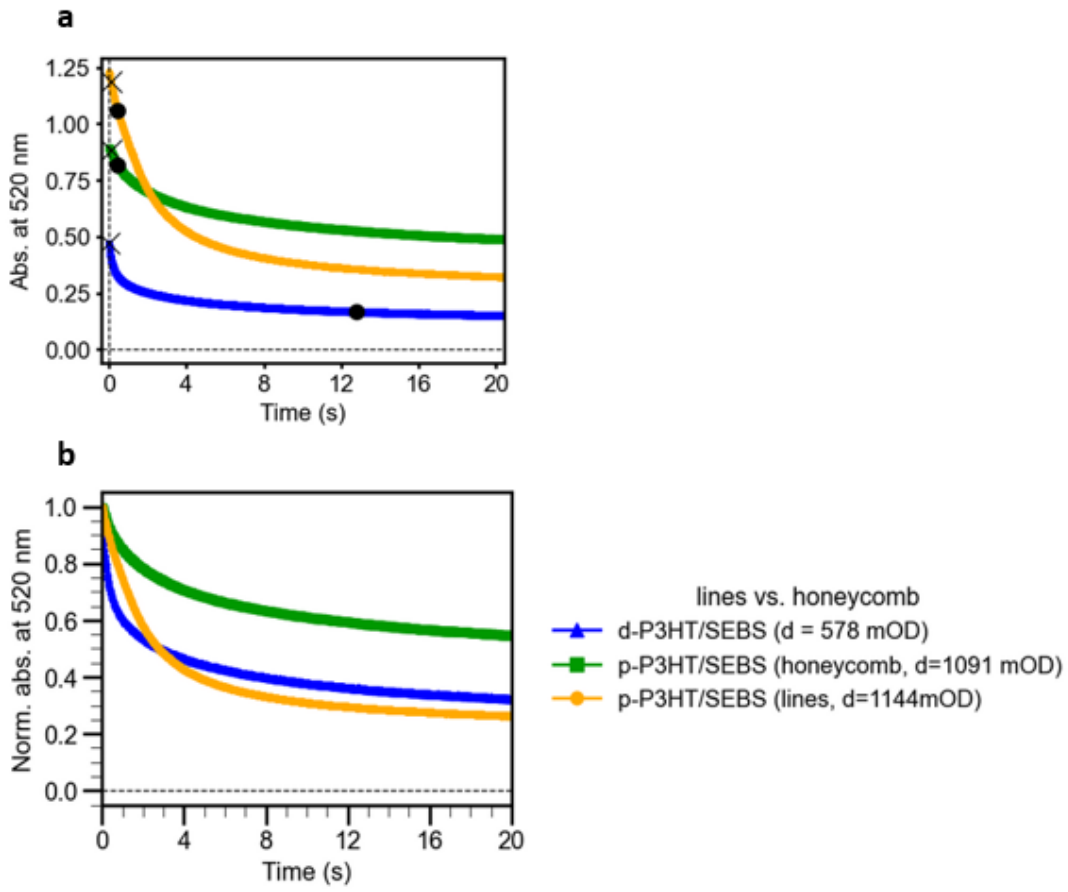

Figure 33. Temporal evolution of the absorbance at 520 nm (neutral peak of P3HT, wavelength sampling) upon P3HT doping at -0.8 V. a) raw data b) normalized data of d-P3HT/SEBS, p-P3HT/SEBS (honeycomb pore structure), p-P3HT/SEBS (linear pore structure).

Unlike the comparisons made on p-P3HT films based on the spin-coating method, both porous films in this case are semi-crystalline (Figure 34). This means that the faster doping rate of the p-P3HT/SEBS film with linear pores, compared to the p-P3HT/SEBS film with a honeycomb structure, cannot be attributed to differences in crystallinity. The enhanced kinetic performance with lines is clear but the reason remains unclear. One possible explanation could be the poor homogeneity of both samples, which could affect the result. Alternatively, the electrons might be forced to follow specific pathways, leading to higher electron mobility and, consequently, faster doping kinetics.

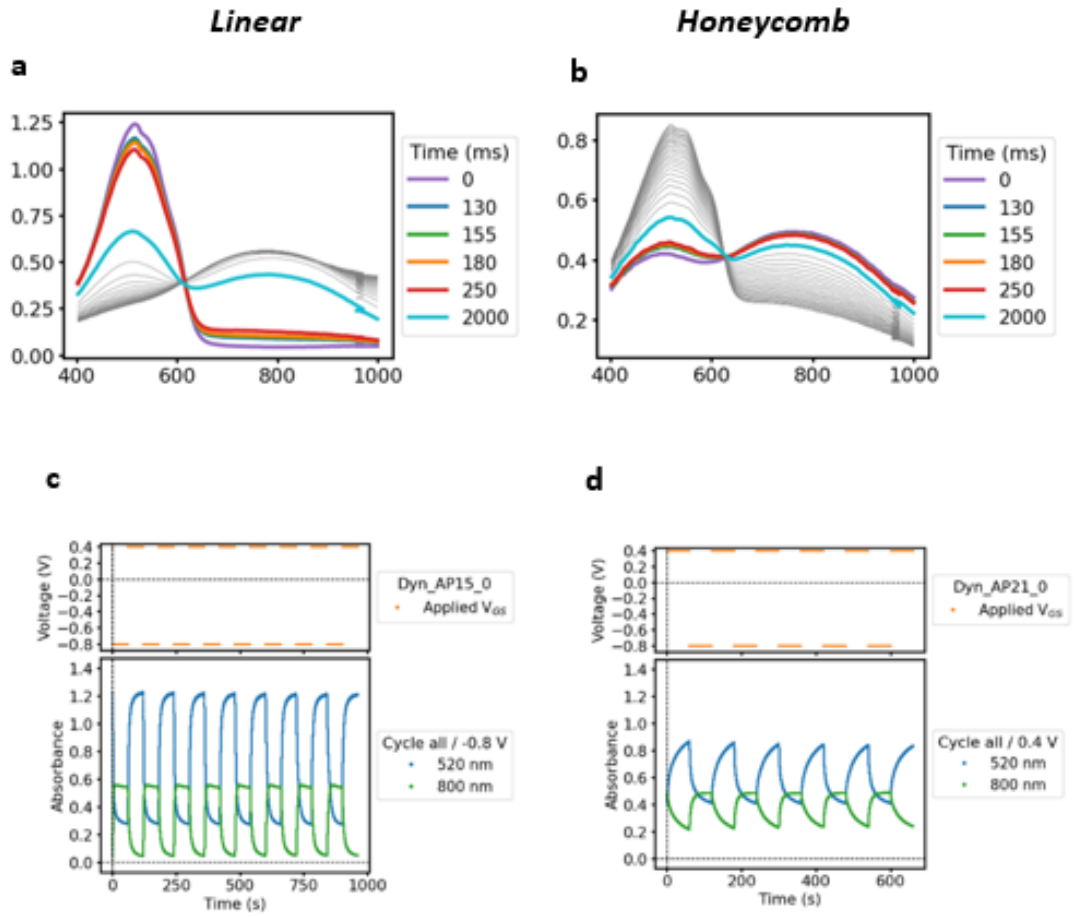

Figure 34. a-b) Evolution over time of Vis-NIR absorbance spectra upon doping at -0.8 V for (left) line and (right) honeycomb pores arrangements. and c-d) Temporal evolution of the absorbance at 520 nm (neutral peak) and 800 nm (polaronic peak) upon P3HT doping at -0.8 V and dedoping at +0.4 V of Linear and Honeycomb pore structure respectively; 10 cycles, dwell$_{ON/OFF}$ =60/60s.

4. CONCLUSIONS

Organic electrochemical transistors (OECTs) have attracted significant attention due to their *low-cost fabrication* and unique set of properties. These include *low operating voltages, mixed conduction properties* (ionic and electric mobility) and *high transconductance,* which makes them especially suitable for bioelectronics applications. However, a key limitation of OECTs is their low kinetic performance. Improving the doping kinetic rate would greatly enhance the device sensitivity, allowing it to detect fast biological events and chemical reactions.[21,24]

This thesis aimed to improve the kinetic performance of OECTs by modifying the morphology of the semiconducting polymeric channel, specifically poly (3-hexylthiophene) (P3HT), through the introduction of porosity. Porous P3HT films were successfully fabricated using the Breath Figure method. By adjusting some parameters such as *SEBS presence , relative humidity, solvent, concentration* and *spin coating method*, the control of pore size, coverage, and arrangement was possible. Optimal conditions included SEBS/P3HT 2:1 ratio, 90% RH, a 92:8 vol% Chloroform:Methanol mixture, a two-step spin coating (2000 rpm for 2 s, 1500 rpm for 90 s), and off-center spin coating method.

The kinetic performance of porous P3HT films compared to the correlative dense films was evaluated by using the time-resolved spectroelectrochemical analysis. The time-resolved spectroelectrochemical analysis was conducted in a sandwich cell configuration with 0.1 mol L-1 aqueous potassium hexafluorophospahte (KPF6) electrolyte, a doping gate voltage of -0.8V and a dedoping gate voltage of 0.4V. Unexpectedly, the results showed that the introduction of porosity did not significantly improve doping kinetics. In fact, dense films exhibited faster doping rates compared to their porous counterparts. An inverse relationship between pore coverage and doping speed was also observed, with less porous films demonstrating faster kinetics. However, these phenomena are primarily attributed to differences in film thickness rather than porosity itself. The dense films were thinner, which allowed for quicker ion transport and, consequently, faster doping. Additionally, the morphological analysis revealed that dense films were semi-crystalline, while the porous films were predominantly amorphous. This distinction in crystallinity further enhanced the doping performance of the dense films, as crystallinity typically improves electron mobility, thereby accelerating the doping process.

Finally, films with a linear pore arrangement exhibited significantly faster doping kinetics compared to those with a honeycomb structure. A plausible explanation is that the linear

arrangement may create more defined pathways for electron flow, enhancing electron mobility and thus speeding up the doping process.

Despite the slower doping kinetics of the porous P3HT films, this research successfully identified and refined an effective method for fabricating porous films. This represents a critical foundation for future efforts to optimize the morphology of semiconducting polymer films, with the aim of improving OECT performance and advancing their potential in bioelectronic applications.

5. REFERENCES

[1] L. Lan, J. Chen, Y. Wang, P. Li, Y. Yu, G. Zhu, Z. Li, T. Lei, W. Yue, I. McCulloch, *Chem. Mater.* **2022**, *34*, 1666–1676.

[2] A. V. Marquez, N. McEvoy, A. Pakdel, *Molecules* **2020**, *25*, 5288.

[3] J. Rivnay, P. Leleux, M. Ferro, M. Sessolo, A. Williamson, D. A. Koutsouras, D. Khodagholy, M. Ramuz, X. Strakosas, R. M. Owens, C. Benar, J.-M. Badier, C. Bernard, G. G. Malliaras, *Sci. Adv.* **2015**, *1*, e1400251.

[4] Z. Zhao, Z. Tian, F. Yan, *Cell Rep. Phys. Sci.* **2023**, *4*, 101673.

[5] J. Rivnay, S. Inal, A. Salleo, R. M. Owens, M. Berggren, G. G. Malliaras, *Nat. Rev. Mater.* **2018**, *3*, 17086.

[6] Y. Wang, Y. Liu, *Trends Chem.* **2023**, *5*, 279–294.

[7] S. Datta, *Interface Mag.* **2013**, *22*, 41–46.

[8] M. Sophocleous, L. Contat-Rodrigo, E. Garcia-Breijo, J. Georgiou, *IEEE Sens. J.* **2021**, *21*, 3977–4006.

[9] M. Ates, *Mater. Sci. Eng. C* **2013**, *33*, 1853–1859.

[10] J. Liao, H. Si, X. Zhang, S. Lin, *Sensors* **2019**, *19*, 218.

[11] S. M. Sze, K. K. Ng, *Physics of Semiconductor Devices*, Wiley-Interscience, Hoboken, N.J, **2007**.

[12] A. Makhinia, L. Bynens, A. Goossens, J. Deckers, L. Lutsen, K. Vandewal, W. Maes, V. Beni, P. Andersson Ersman, *Adv. Funct. Mater.* **2024**, *34*, 2314857.

[13] M. Moser, J. F. Ponder, A. Wadsworth, A. Giovannitti, I. McCulloch, *Adv. Funct. Mater.* **2019**, *29*, 1807033.

[14] P. R. Paudel, V. Kaphle, D. Dahal, R. K. Radha Krishnan, B. Lüssem, *Adv. Funct. Mater.* **2021**, *31*, 2004939.

[15] H. Shen, C.-A. Di, D. Zhu, *Sci. China Chem.* **2017**, *60*, 437–449.

[16] H. Guo, C. Liu, Y. Peng, L. Gao, J. Yu, *Sensors* **2023**, *23*, 6910.

[17] Y. Peng, L. Gao, C. Liu, J. Deng, M. Xie, L. Bai, G. Wang, Y. Cheng, W. Huang, J. Yu, *Nano Res.* **2023**, *16*, 10206–10214.

[18] H. Jia, Z. Huang, P. Li, S. Zhang, Y. Wang, J.-Y. Wang, X. Gu, T. Lei, *J. Mater. Chem. C* **2021**, *9*, 4927–4934.

[19] P. Li, T. Lei, *J. Polym. Sci.* **2022**, *60*, 377–392.

[20] H. S. White, G. P. Kittlesen, M. S. Wrighton, *J. Am. Chem. Soc.* **1984**, *106*, 5375–5377.

[21] A. Ait Yazza, P. Blondeau, F. J. Andrade, *ACS Appl. Electron. Mater.* **2021**, *3*, 1886–1895.

[22] D. A. Koutsouras, F. Torricelli, P. W. M. Blom, *Adv. Electron. Mater.* **2023**, *9*, 2200868.

[23] D. Khodagholy, J. Rivnay, M. Sessolo, M. Gurfinkel, P. Leleux, L. H. Jimison, E. Stavrinidou, T. Herve, S. Sanaur, R. M. Owens, G. G. Malliaras, *Nat. Commun.* **2013**, *4*, 2133.

[24] D. Ohayon, V. Druet, S. Inal, *Chem. Soc. Rev.* **2023**, *52*, 1001–1023.

[25] X. Wu, A. Surendran, M. Moser, S. Chen, B. T. Muhammad, I. P. Maria, I. McCulloch, W. L. Leong, *ACS Appl. Mater. Interfaces* **2020**, *12*, 20757–20764.

[26] Y. He, N. A. Kukhta, A. Marks, C. K. Luscombe, *J. Mater. Chem. C* **2022**, *10*, 2314–2332.

[27] M. Xie, H. Liu, M. Wu, C. Chen, J. Wen, L. Bai, J. Yu, W. Huang, *Org. Electron.* **2023**, *117*, 106777.

[28] L. Q. Flagg, R. Giridharagopal, J. Guo, D. S. Ginger, *Chem. Mater.* **2018**, *30*, 5380–5389.

[29] J. T. Friedlein, M. J. Donahue, S. E. Shaheen, G. G. Malliaras, R. R. McLeod, *Adv. Mater.* **2016**, *28*, 8398–8404.

[30] J. Chen, W. Huang, D. Zheng, Z. Xie, X. Zhuang, D. Zhao, Y. Chen, N. Su, H. Chen, R. M. Pankow, Z. Gao, J. Yu, X. Guo, Y. Cheng, J. Strzalka, X. Yu, T. J. Marks, A. Facchetti, *Nat. Mater.* **2022**, *21*, 564–571.

[31] G. D. Spyropoulos, J. N. Gelinas, D. Khodagholy, *Sci. Adv.* **2019**, *5*, DOI 10.1126/sciadv.aau7378.

[32] S. E. Chen, L. Q. Flagg, J. W. Onorato, L. J. Richter, J. Guo, C. K. Luscombe, D. S. Ginger, *J. Mater. Chem. A* **2022**, *10*, 10738–10749.

[33] S. R. Jackson, R. L. Kingsford, G. W. Collins, C. G. Bischak, *Chem. Mater.* **2023**, *35*, 5392–5400.

[34] P. Cavassin, I. Holzer, D. Tsokkou, O. Bardagot, J. Réhault, N. Banerji, *Adv. Mater.* **2023**, *35*, 2300308.

[35] P. R. Paudel, J. Tropp, V. Kaphle, J. D. Azoulay, B. Lüssem, *J. Mater. Chem. C* **2021**, *9*, 9761–9790.

[36] B. Meng, J. Liu, L. Wang, *Polym. Chem.* **2020**, *11*, 1261–1270.

[37] M. Moser, L. R. Savagian, A. Savva, M. Matta, J. F. Ponder, T. C. Hidalgo, D. Ohayon, R. Hallani, M. Reisjalali, A. Troisi, A. Wadsworth, J. R. Reynolds, S. Inal, I. McCulloch, *Chem. Mater.* **2020**, *32*, 6618–6628.

[38] Lucas Q. Flagg, C. G. Bischak, J. W. Onorato, R. B. Rashid, C. K. Luscombe, D. S. Ginger, *J. Am. Chem. Soc.* **2019**, *141*, 4345–4354.

[39] L. Huang, Z. Wang, J. Chen, B. Wang, Y. Chen, W. Huang, L. Chi, T. J. Marks, A. Facchetti, *Adv. Mater.* **2021**, *33*, 2007041.

[40] X. Zhang, B. Wang, L. Huang, W. Huang, Z. Wang, W. Zhu, Y. Chen, Y. Mao, A. Facchetti, T. J. Marks, *Sci. Adv.* **2020**, *6*, eaaz1042.

[41] R. Giridharagopal, J. Guo, J. Kong, D. S. Ginger, *ACS Appl. Mater. Interfaces* **2021**, *13*, 34616–34624.

[42] E. Bormashenko, *Membranes* **2017**, *7*, 45.

[43] M.-S. Yuan, W. Xu, Q.-G. He, J.-G. Cheng, Y.-Y. Fu, *Chin. J. Anal. Chem.* **2022**, *50*, 44–52.

[44] H. Yabu, *Sci. Technol. Adv. Mater.* **2018**, *19*, 802–822.

[45] A. Zhang, H. Bai, L. Li, *Chem. Rev.* **2015**, *115*, 9801–9868.

[46] W. Liu, C. Li, X. Lin, H. Xie, Y. Chen, Z. Li, G. Zeng, *Cellulose* **2022**, *29*, 6463–6491.

[47] Y. Dou, M. Jin, G. Zhou, L. Shui, *Membranes* **2015**, *5*, 399–424.

[48] E. Ferrari, P. Fabbri, F. Pilati, *Langmuir* **2011**, *27*, 1874–1881.

[49] P. Escalé, L. Rubatat, L. Billon, M. Save, *Eur. Polym. J.* **2012**, *48*, 1001–1025.

[50] M. S. Park, J. K. Kim, *Langmuir* **2004**, *20*, 5347–5352.

[51] W. Madej, A. Budkowski, J. Raczkowska, J. Rysz, *Langmuir* **2008**, *24*, 3517–3524.

[52] Y.-K. Hong, H. Kim, G. Lee, W. Kim, J.-I. Park, J. Cheon, J.-Y. Koo, *Appl. Phys. Lett.* **2002**, *80*, 844–846.

[53] N. Hedayat, Y. Du, H. Ilkhani, *Renew. Sustain. Energy Rev.* **2017**, *77*, 1221–1239.

[54] J. Danglad-Flores, K. Eftekhari, A. G. Skirtach, H. Riegler, *Langmuir* **2019**, *35*, 3404–3412.

[55] M. D. Tyona, *Adv. Mater. Res.* **2013**, *2*, 195–208.

[56] Y. Mouhamad, P. Mokarian-Tabari, N. Clarke, R. A. L. Jones, M. Geoghegan, *J. Appl. Phys.* **2014**, *116*, 123513.

[57] Y. Yuan, G. Giri, A. L. Ayzner, A. P. Zoombelt, S. C. B. Mannsfeld, J. Chen, D. Nordlund, M. F. Toney, J. Huang, Z. Bao, *Nat. Commun.* **2014**, *5*, 3005.

[58] E. Laborda, J. García-Martínez, A. Molina, *Electrochem. Commun.* **2021**, *123*, 106915.

[59] J. J. A. Lozeman, P. Führer, W. Olthuis, M. Odijk, *The Analyst* **2020**, *145*, 2482–2509.

[60] Y. Kobayashi, A. Odo, *J. Mater. Res. Technol.* **2014**, *3*, 290–295.

[61] A. Das, A. B. Dey, S. Chattopadhyay, G. De, M. K. Sanyal, R. Mukherjee, *Langmuir* **2020**, *36*, 15270–15282.

[62] L. Van Tho, W.-T. Park, E.-Y. Choi, Y.-Y. Noh, *Appl. Phys. Lett.* **2017**, *110*, 163303.

[63] C. Liu, M. Wu, L. Gao, H. Liu, J. Yu, *Sens. Actuators B Chem.* **2022**, *371*, 132540.

[64] L. Gao, C. Liu, Y. Peng, J. Deng, S. Hou, Y. Cheng, W. Huang, J. Yu, *Sens. Actuators B Chem.* **2022**, *368*, 132113.

[65] M. Roesing, J. Howell, D. Boucher, *J. Polym. Sci. Part B Polym. Phys.* **2017**, *55*, 1075–1087.

[66] D. T. Duong, B. Walker, J. Lin, C. Kim, J. Love, B. Purushothaman, J. E. Anthony, T. Nguyen, *J. Polym. Sci. Part B Polym. Phys.* **2012**, *50*, 1405–1413.

[67] G. Ovejero, P. Pérez, M. D. Romero, I. Díaz, E. Díez, *Eur. Polym. J.* **2009**, *45*, 590–594.

[68] H. Yabu, Y. Hirai, M. Shimomura, *Langmuir* **2006**, *22*, 9760–9764.

[69] W. Dong, Y. Zhou, D. Yan, Y. Mai, L. He, C. Jin, *Langmuir* **2009**, *25*, 173–178.

[70] M. S. Park, W. Joo, J. K. Kim, *Langmuir* **2006**, *22*, 4594–4598.

[71] R. Ghosh, A. R. Chew, J. Onorato, V. Pakhnyuk, C. K. Luscombe, A. Salleo, F. C. Spano, *J. Phys. Chem. C* **2018**, *122*, 18048–18060.